

NASA/TM–2014-104606/Vol. 37



Technical Report Series on Global Modeling and Data Assimilation, Volume 37

Randal D. Koster, Editor

Maintaining Atmospheric Mass and Water Balance Within Reanalysis

Lawrence L. Takacs, Max Suarez, and Ricardo Todling

National Aeronautics and
Space Administration

Goddard Space Flight Center
Greenbelt, Maryland 20771

March 2015

NASA STI Program ... in Profile

Since its founding, NASA has been dedicated to the advancement of aeronautics and space science. The NASA scientific and technical information (STI) program plays a key part in helping NASA maintain this important role.

The NASA STI program operates under the auspices of the Agency Chief Information Officer. It collects, organizes, provides for archiving, and disseminates NASA's STI. The NASA STI program provides access to the NASA Aeronautics and Space Database and its public interface, the NASA Technical Report Server, thus providing one of the largest collections of aeronautical and space science STI in the world. Results are published in both non-NASA channels and by NASA in the NASA STI Report Series, which includes the following report types:

- **TECHNICAL PUBLICATION.** Reports of completed research or a major significant phase of research that present the results of NASA Programs and include extensive data or theoretical analysis. Includes compilations of significant scientific and technical data and information deemed to be of continuing reference value. NASA counterpart of peer-reviewed formal professional papers but has less stringent limitations on manuscript length and extent of graphic presentations.
- **TECHNICAL MEMORANDUM.** Scientific and technical findings that are preliminary or of specialized interest, e.g., quick release reports, working papers, and bibliographies that contain minimal annotation. Does not contain extensive analysis.
- **CONTRACTOR REPORT.** Scientific and technical findings by NASA-sponsored contractors and grantees.
- **CONFERENCE PUBLICATION.** Collected papers from scientific and technical conferences, symposia, seminars, or other meetings sponsored or co-sponsored by NASA.
- **SPECIAL PUBLICATION.** Scientific, technical, or historical information from NASA programs, projects, and missions, often concerned with subjects having substantial public interest.
- **TECHNICAL TRANSLATION.** English-language translations of foreign scientific and technical material pertinent to NASA's mission.

Specialized services also include organizing and publishing research results, distributing specialized research announcements and feeds, providing help desk and personal search support, and enabling data exchange services. For more information about the NASA STI program, see the following:

- Access the NASA STI program home page at <http://www.sti.nasa.gov>
 - E-mail your question via the Internet to help@sti.nasa.gov
 - Fax your question to the NASA STI Help Desk at 443-757-5803
 - Phone the NASA STI Help Desk at 443-757-5802
 - Write to:
NASA STI Help Desk
NASA Center for AeroSpace Information
7115 Standard Drive
Hanover, MD 21076-1320
-



**Technical Report Series on Global Modeling and Data Assimilation,
Volume 37**

Randal D. Koster, Editor

**Maintaining Atmospheric Mass and Water Balance Within
Reanalysis**

Lawrence L. Takacs

NASA's Goddard Space Flight Center, Greenbelt, Maryland

Max Suarez

NASA's Goddard Space Flight Center, Greenbelt, Maryland

Ricardo Todling

NASA's Goddard Space Flight Center, Greenbelt, Maryland

National Aeronautics and
Space Administration

**Goddard Space Flight Center
Greenbelt, Maryland 20771**

Notice for Copyrighted Information

This manuscript is a work of the United States Government authored as part of the official duties of employee(s) of the National Aeronautics and Space Administration. No copyright is claimed in the United States under Title 17, U.S. Code. All other rights are reserved by the United States Government. Any publisher accepting this manuscript for publication acknowledges that the United States Government retains a nonexclusive, irrevocable, worldwide license to prepare derivative works, publish or reproduce the published from of this manuscript, or allow others to do so, for United States Government purposes.

Trade names and trademarks are used in this report for identification only. Their usage does not constitute an official endorsement, either expressed or implied, by the National Aeronautics and Space Administration.

Level of Review: This material has been technically reviewed by technical management

Available from:
NASA Center for AeroSpace Information
7115 Standard Drive
Hanover, MD 21076-1320

National Technical Information Service
5285 Port Royal Road
Springfield, VA 22161 Price Code: A17

Abstract

This report describes the modifications implemented into the Goddard Earth Observing System Version-5 (GEOS-5) Atmospheric Data Assimilation System (ADAS) to maintain global conservation of dry atmospheric mass as well as to preserve the model balance of globally integrated precipitation and surface evaporation during reanalysis. Section 1 begins with a review of these global quantities from four current reanalysis efforts. Section 2 introduces the modifications necessary to preserve these constraints within the atmospheric general circulation model (AGCM), the Gridpoint Statistical Interpolation (GSI) analysis procedure, and the Incremental Analysis Update (IAU) algorithm. Section 3 presents experiments quantifying the impact of the new procedure. Section 4 shows preliminary results from its use within the GMAO MERRA-2 Reanalysis project. Section 5 concludes with a summary.

1) Introduction

A key goal of recent atmospheric reanalysis efforts has been to extract statistically significant signals from within Data Assimilation System (DAS) products that are relevant to climate change. By using the most scientifically advanced but “frozen” systems during reanalysis, we expect to remove the impact of improved model physics and/or dynamics over time and hopefully more clearly determine trends in the actual climate based on the assimilated observational record. For example, trends in global surface temperature should be detected by trends in globally integrated water content and the associated estimates of precipitation and surface evaporation. Complicating this scenario, however, are changes in observational instrument and satellite technology over the reanalysis period and the model response associated with those changes. As noted in Bosilovich and Robertson (2011), the latest reanalyses are still significantly impacted by changes in the observing system with regard to globally integrated precipitation estimates. Figure 1.1 shows the time series of the globally integrated evaporation (E) and precipitation (P) from four existing reanalyses: 1) MERRA (Rienecker et al., 2011), 2) ERA-Interim (Dee et al., 2011), 3) JRA-55 (Ebata et al., 2011), and 4) NCEP-CFSR (Saha et al., 2010). We clearly see imbalances between P and E from all four cases that may or may not be physically linked to changes in total atmospheric water content. Imbalances are of both signs and can even change sign within a single reanalysis. Changes in the globally integrated precipitation tend, in general, to be more volatile than globally integrated evaporation, and they may be more susceptible to changes in atmospheric water vapor content due to changes in the observational satellite database over time.

In addition to global estimates of precipitation, there is also considerable interest in the estimate of total atmospheric mass (e.g., Trenberth and Smith, 2005; Hoinka, 1998; Trenberth and Guillemot, 1994; Trenberth, 1991; Trenberth et al., 1987). As suggested by Trenberth and Smith (2005), the total mass of the atmosphere can and *should* be utilized as a constraint in global analyses in addition to being of interest in its own right. As they and the other studies have pointed out, the globally integrated dry atmospheric mass to first order should be conserved (ignoring such effects as burning of fossil fuels, anthropogenic sources and sinks, the outgassing in volcanoes, and loss to space). In each of the four reanalyses in Fig. 1.1, however, there is no fundamental mechanism to ensure that resulting analyzed states maintain conservation of globally integrated dry atmospheric mass. Conservation of dry mass implies that there is a consistent relationship between changes in total mass and changes in total water content.

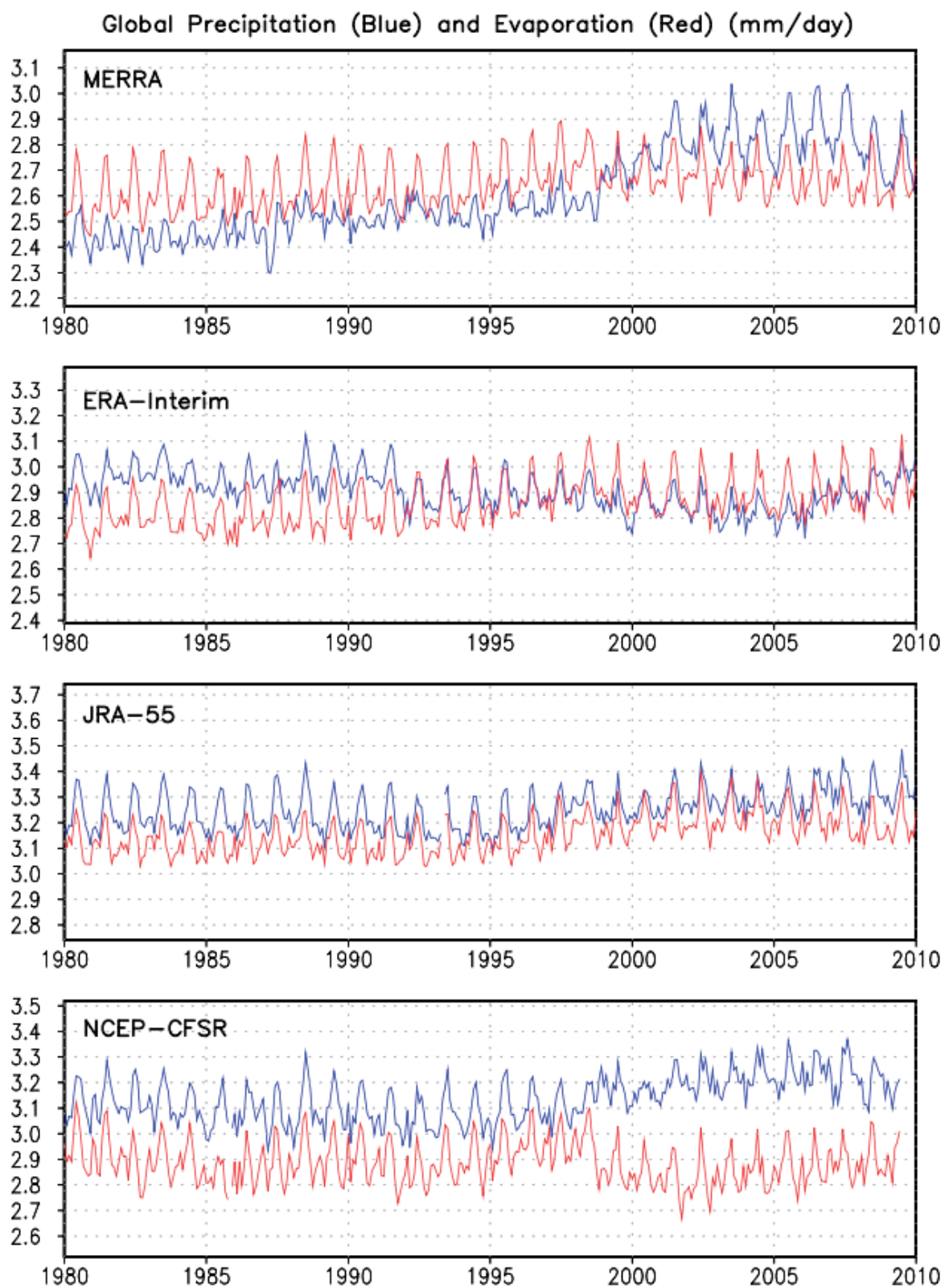


Figure 1.1: Monthly mean globally integrated precipitation and surface evaporation from MERRA, ERA-Interim, JRA-55, and NCEP-CFSR Reanalyses.

For our purposes we define total mass (in units of hydrostatic pressure) as simply the sum of the atmospheric dry mass plus the mass of the total water content:

$$P_{TOT} = P_{DRY} + P_{WET} ,$$

$$P_{TOT} = \int_{p_{surf}}^{p_{top}} dp ,$$

$$P_{WET} = \int_{p_{surf}}^{p_{top}} q_W dp ,$$

where q_W is the total water content defined as the sum of the vapor, liquid, and frozen components:

$$q_W = q_V + q_L + q_I ,$$

and q_k is the specific mass of constituent k . Figure 1.2 shows the time series from the four reanalyses of the climatological seasonal cycle of total water content and their corresponding monthly-mean time tendency, in addition to the monthly mean total water content anomalies. The climatological seasonal cycles of total water content are all well analyzed, with small variations in magnitude of the annual mean values between the reanalyses. The climatological time tendencies of total water content, however, are virtually identical. With regard to the monthly mean anomalies, there is a high degree of correlation between MERRA and NCEP-CFSR, while ERA-Interim and JRA-55 are more closely related. The MERRA and NCEP-CFSR anomalies show a distinct rise in total water content over the reanalysis period, which is consistent with the general rise in the prescribed temperatures used as boundary conditions during the reanalysis.

To delineate more clearly the imbalance between E and P, Figure 1.3 compares the *implied* model-generated globally-integrated water tendency (i.e., E-minus-P, or E-P) on the same scale as the actual tendency of globally integrated assimilated water vapor. We see that the implied water vapor tendency from the model derived E-P residual is much larger than the actual water vapor tendency. Assuming that the models used in the reanalyses contain no spurious sources or sinks of water content, the imbalance between the implied water vapor tendency (E-P) and the actual water vapor tendency must be due to water added or removed by the analysis.

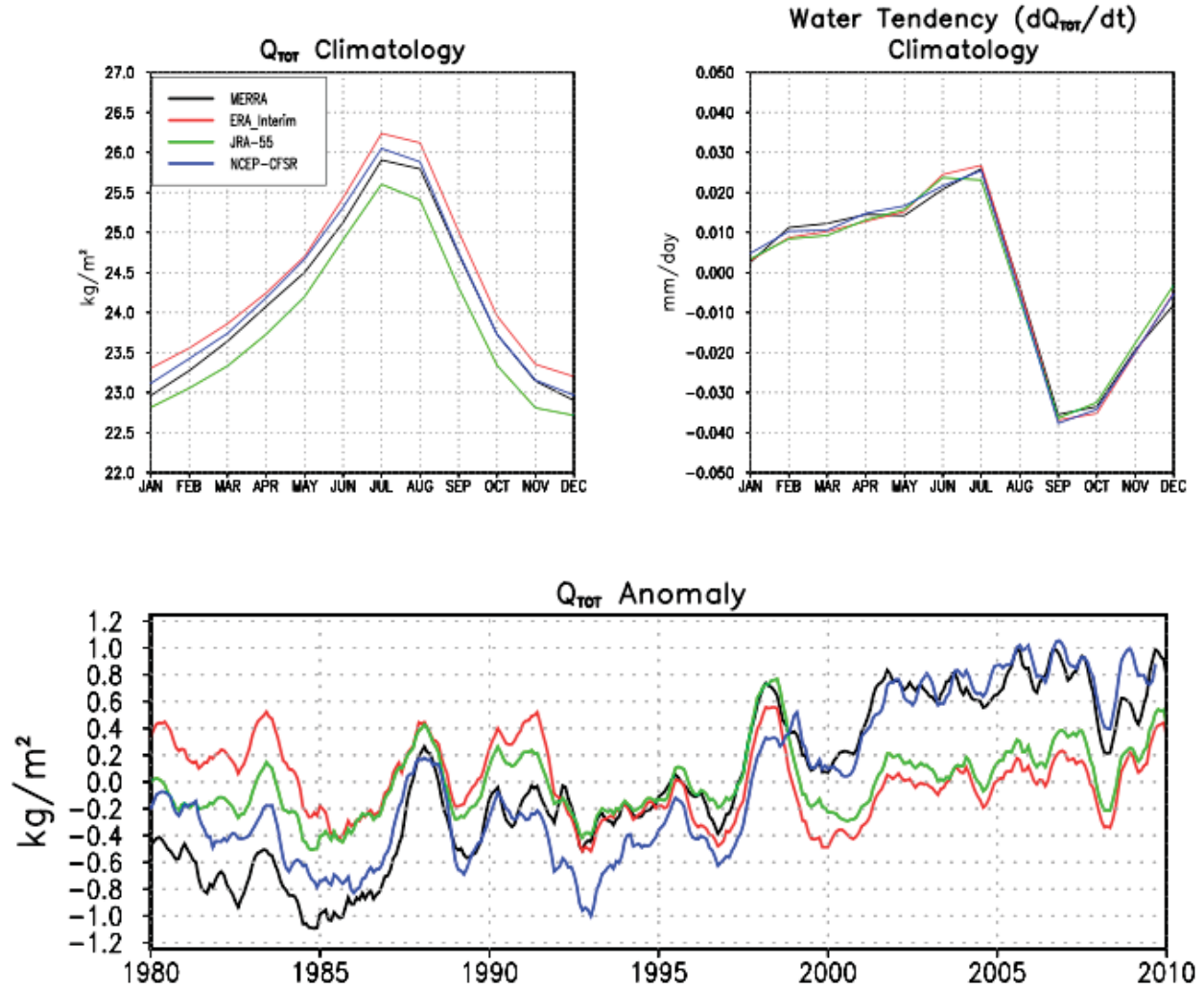


Figure 1.2: Climatologies of total water content (top left) and tendency (top right), plus the total water content anomaly (bottom) from MERRA, ERA-Interim, JRA-55, and NCEP-CFSR Reanalyses.

As noted earlier, to conserve globally integrated dry mass there must be a physically consistent relationship between changes in total mass and changes in total water content. We have seen, however, that the four reanalyses violate the consistency of implied total water content tendency (through E-P) compared with actual assimilated total water tendency. This gives rise to questions regarding the system's total mass and its separation into dry and wet components. Figure 1.4 shows the time series of the climatological seasonal cycle of total mass (in terms of surface pressure) as well as the monthly mean anomalies from the four reanalyses. In addition we show the time series of the dry and wet components separately. The climatological seasonal cycle of total mass clearly reflects the seasonal cycle of total water content. However, the magnitudes of the annual mean values vary substantially between the reanalyses. Most disturbing is the lack of conservation of dry mass and the high correlation between the total

and dry mass anomalies rather than between the total and wet anomalies. The lack of dry mass conservation and the imbalance between globally integrated P and E from all four reanalyses are physically unrealistic; these problems serve as motivation to improve the GMAO Atmospheric Data Assimilation System (ADAS) for the upcoming GMAO MERRA-2 reanalysis.

2) Modifications to Model and Analysis

2a) Adjustment to the model's mass balance:

As shown in Section (1), the reanalysis products from all centers exhibit a fairly consistent representation of the seasonal cycle of total mass due to the seasonal cycle of total water content. In the MERRA system this was driven completely by the analyzed surface pressure since the GEOS-5 AGCM had no pressure change due to changes in water content from moist physics. Further, since conservation of total mass is guaranteed in the dynamical core, all time fluctuations of total mass are due to the analysis increment of surface pressure. Therefore, as a first step toward the development of physically-based dry mass conservation, the AGCM had to be modified to incorporate changes in total pressure due to changes in water content from the moist physics.

In the GEOS-5 AGCM, moist physics parameterizations consist of time tendencies of specific humidity (in the form of vapor: q_{vap} , liquid: q_{liq} , and ice: q_{ice}) due to contributions from convection and large-scale rain, from turbulence, and from stratospheric chemistry. In the model used for MERRA, these parameterizations preserve the mass of each layer, $\frac{\Delta p}{g}$. This behavior is retained in the new model but a correction is made to the layer masses to properly account for the mass change due to evaporation and precipitation:

$$\frac{\Delta p^a}{g} = \frac{\Delta p^b}{g} [1 + (\tilde{q}_w - q_w^b)],$$

where \tilde{q}_w is the specific mass of total water produced by the physics, and the superscripts b and a indicate quantities *before* and *after* the mass corrections are applied. Finally, a correction is made to the specific masses of *all* constituents, including the water specific masses, to account for total mass changes associated with any change in total water produced by the physics. This correction is done on a layer by layer basis to conserve constituent mass in each layer. If \tilde{q}_k is the specific mass of constituent k upon exiting the physics, it is multiplied by the ratio of the layer masses before and after the change in total water is accounted for:

$$q_k^a = \frac{\Delta p^b}{\Delta p^a} \tilde{q}_k,$$

where $\frac{\Delta p^b}{g} \tilde{q}_k$ is the layer mass of constituent k as the physics left it and is identical to $\frac{\Delta p^a}{g} q_k^a$, the constituent mass after the change in total mass due to water changes and the correction to q_k .

With this modification to the moist physics, the globally integrated time-tendency of the total mass of the atmosphere is governed by the time-tendency of the moist component, thereby leaving the dry mass globally conserved. Since the model now retains whatever initial value it sees, a value must be chosen for the globally integrated dry mass (or surface pressure equivalent) in the model's initial conditions. Trenberth and Smith (2005) documented global dry mass monthly values from three different reanalyses (ERA-40, ERA-15, and NCEP-NCAR) over the period from 1950-2000 to range from 982 to 984 hPa. Figure 2.1 shows the dry surface pressures from the four reanalyses discussed in Section 1. Based on these more recent reanalyses, a value of 983.24 hPa was chosen for initialization of GMAO model initial conditions and the MERRA-2 system.

Using the developments outlined above, Figure 2.2 shows the DJF and JJA seasonal climatologies of the surface pressure tendency due to moist physics from a 30-year ½-deg GEOS-5 AGCM AMIP simulation. We clearly see the decrease of mass associated with precipitation in regions of tropical convection and mid-latitude storm tracks, as well as the increase of mass in regions of surface evaporation and subsidence.

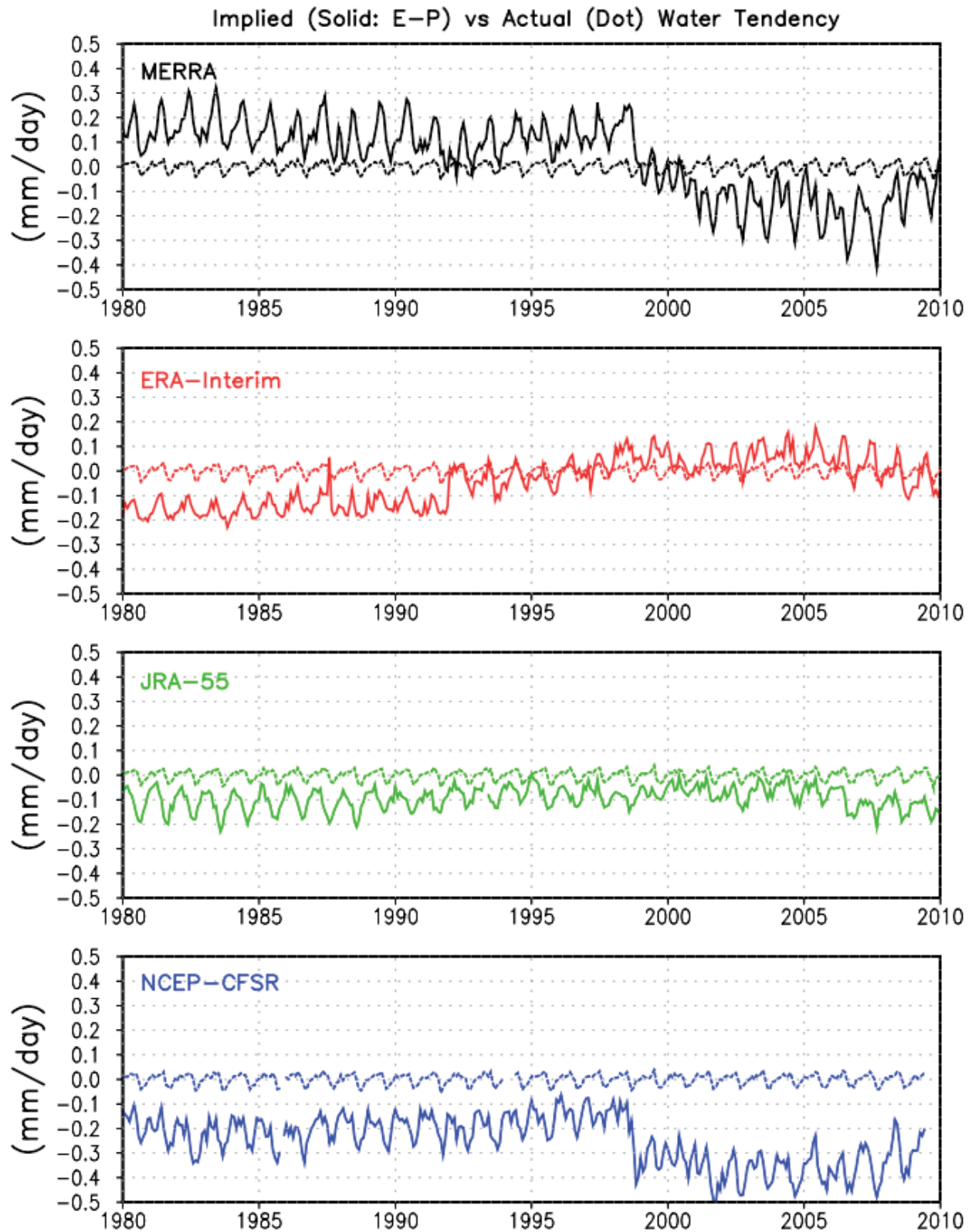


Figure 1.3: Implied (E-P) vs actual monthly mean globally integrated water tendency from MERRA, ERA-Interim, JRA-55, and NCEP-CFSR Reanalyses.

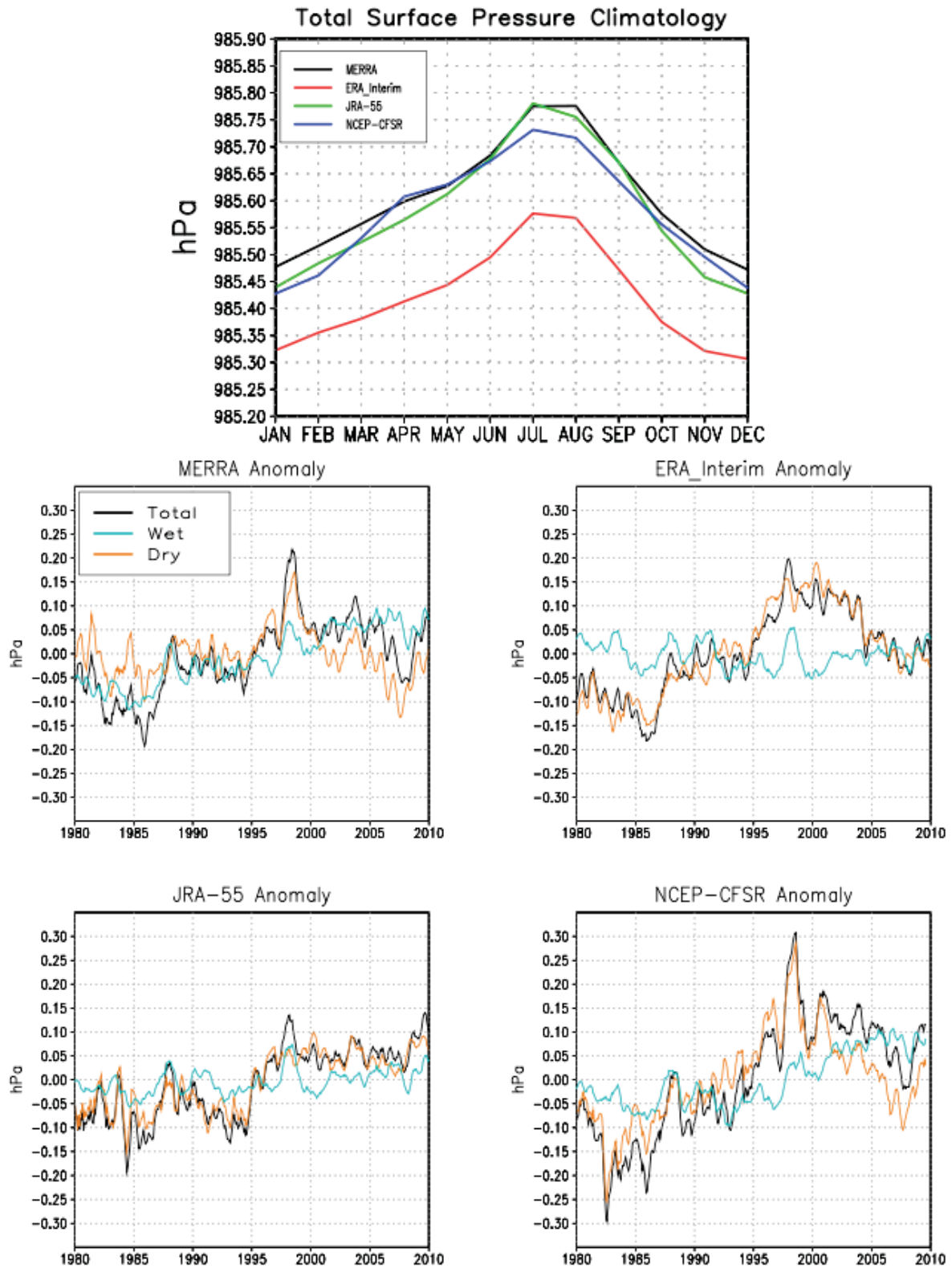


Figure 1.4: Climatology and monthly mean anomalies of globally integrated mass from MERRA, ERA-Interim, JRA-55, and NCEP-CFSR Reanalyses. Also shown is the partition of dry and moist components.

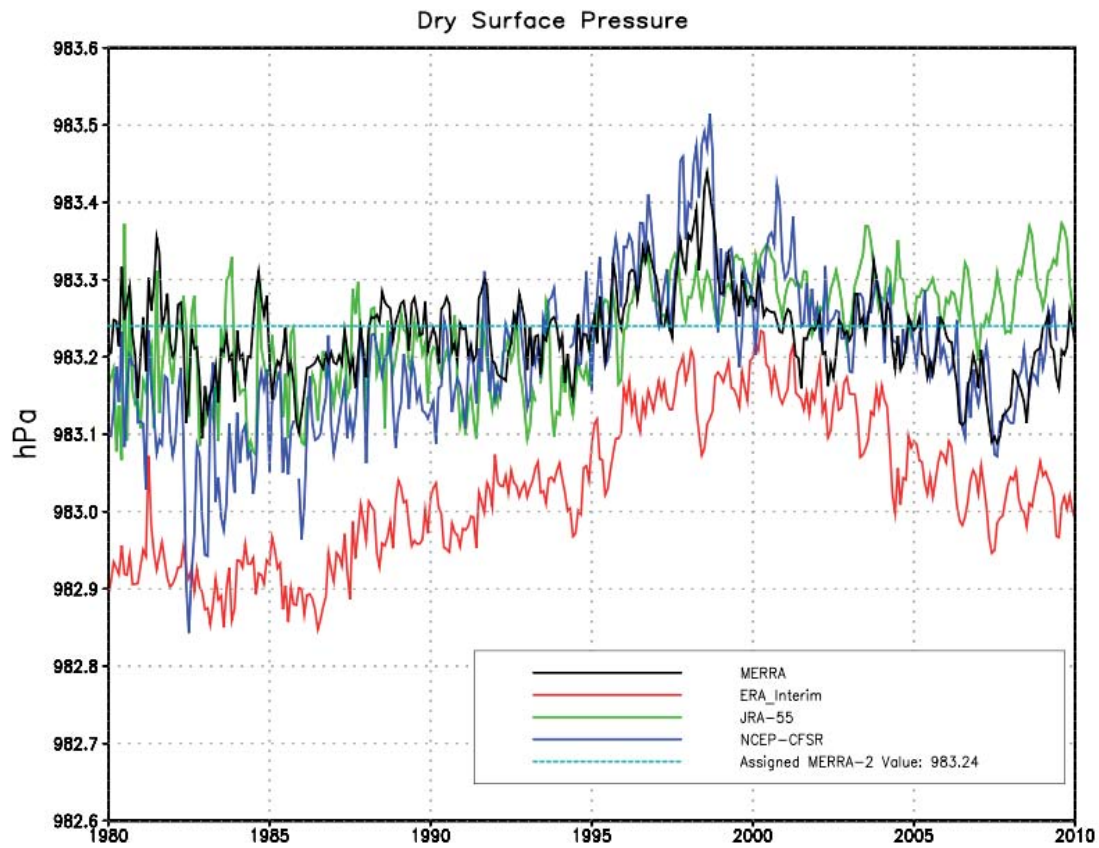


Figure 2.1: Globally integrated dry surface pressure from four reanalyses as well as the value chosen for the MERRA-2 system.

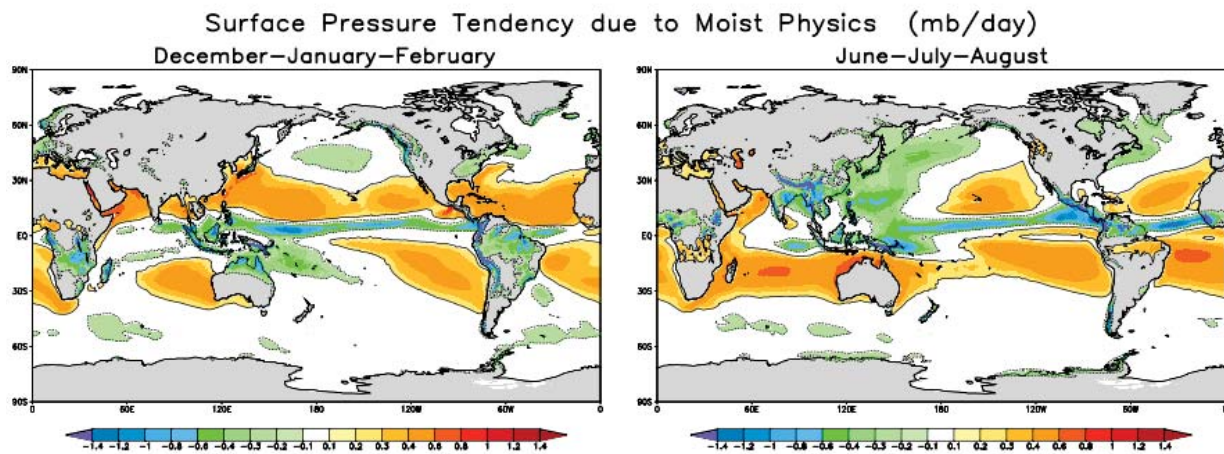


Figure 2.2: Seasonal climatologies of the surface pressure tendency due to moist physics.

Figure 2.3 shows the time-series of globally integrated mass within the 30-year $\frac{1}{2}$ -deg GEOS-5 AGCM AMIP simulation. While the model used for MERRA had no seasonal cycle of total pressure (not shown), Figure 2.3 shows a very realistic climatological seasonal cycle of total pressure which is perfectly correlated with the climatological seasonal cycle of total water content. The 30-year time-series of globally integrated surface pressure anomalies shows that dry mass is perfectly conserved during the run. All trends within the total pressure are solely due to trends within the total water content (total and wet components overlay exactly). It is interesting to note that the trend in total water content is highly correlated (as shown) with the trend in the prescribed 1-deg SST (Reynolds et al., 2002) boundary condition.

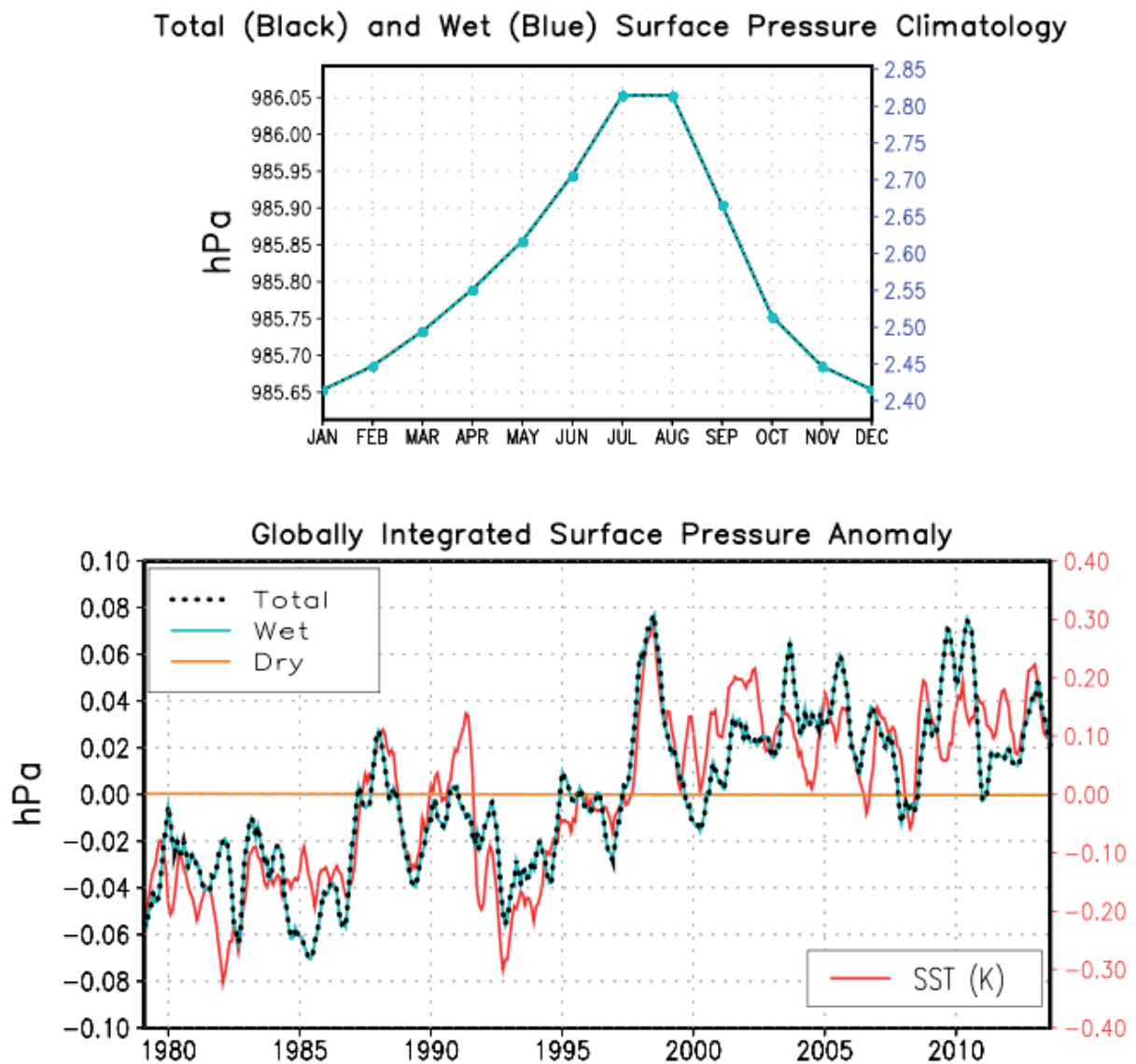


Figure 2.3: Climatology and monthly mean anomalies of globally integrated mass from the GEOS-5 AGCM AMIP simulation. Also shown is the partition of dry and moist components. (Note: SST anomalies (K) are scaled on the right)

Figure 2.4 shows the time-series of globally integrated total precipitation and surface evaporation from the same 30-year GEOS-5 AGCM climate simulation. In this pure model run we see the consistent long-term balance between sources and sinks of total water content. These results show that the updated model includes the necessary improvements needed for dry mass conservation and can maintain proper balance between globally integrated precipitation and evaporation.

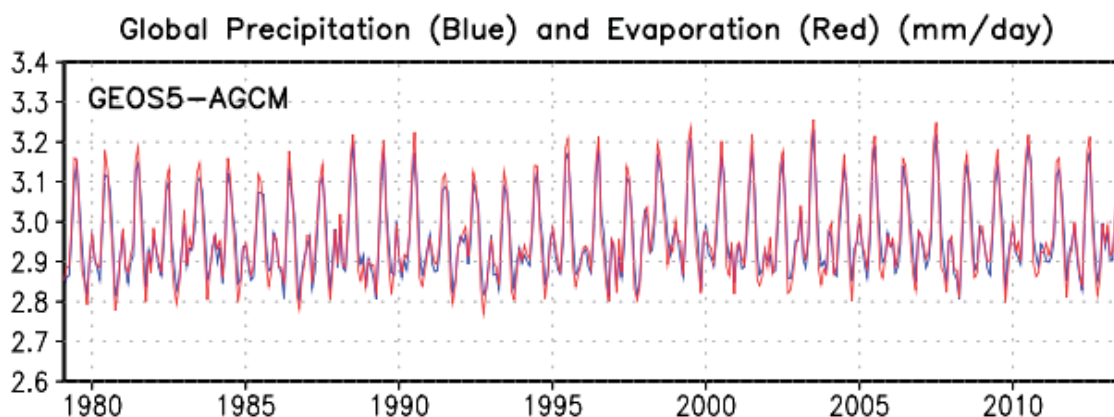


Figure 2.4: Monthly mean globally integrated precipitation and surface evaporation from the GEOS-5 AGCM AMIP simulation.

2b) Additional Analysis Constraint:

If, as discussed earlier, the data assimilation system is expected to conserve total dry mass, not only do we need the AGCM to preserve this quantity, the atmospheric analysis must also be constrained to preserve dry mass. Unlike the version of GSI used for MERRA, the present version of GSI (Kleist et al., 2009) includes a trigger for an additional constraint to penalize changes in dry mass (J. C. Derber and D. T. Kleist, pers. comm.). Originally, this feature was implemented to work within the context of the minimization option that uses the pre-conditioned conjugate gradient (PCG) of Derber and Rosati (1989). However, presently the GEOS-5 ADAS uses the bi-conjugate gradient (BiCG) algorithm of El Akkraoui et al. (2013), which is available as one of the alternative minimization procedures in GSI. The main difference between the PCG and BiCG implementations is in the calculation of the step defining the steepest descent at each iteration of the minimization, with the BiCG using a simple gradient norm ratio which works well when the inner loop of three-dimensional, variational (3D-Var) analysis is linearized, as in GEOS-5 ADAS. The analysis software has then been revised to allow for the dry mass constraint to apply regardless of the minimization procedure employed by GSI.

The implementation of this constraint amounts to introducing an additional term, J_d , to the usual analysis cost function:

$$J = J_b + J_o + J_d,$$

where J_b and J_o represent the typical background and observation cost terms of a first-guess-at-appropriate-time 3D-Var analysis (e.g., see Massart et al., 2010). Explicitly, the term ensuring minimal changes to total dry mass is written as

$$J_d = \gamma (\delta q - \delta q_w)^2$$

where $\delta q = \sum_k \delta q_k \delta A \delta p_k$ is the increment to total mass calculated over all vertical levels of the background; $\delta q_w = \sum_k [\delta q_k^v + \delta q_k^l + \delta q_k^i] \delta A \delta p_k$ is the incremental contribution of vapor, liquid and ice water contents to total mass, with δA and δp_k representing the horizontal and vertical grid weights, respectively; and the parameter γ is used to control the strength of the penalty. Since this term is applied as a weak-constraint to the minimization problem, dry-mass conservation is only *approximately* guaranteed.

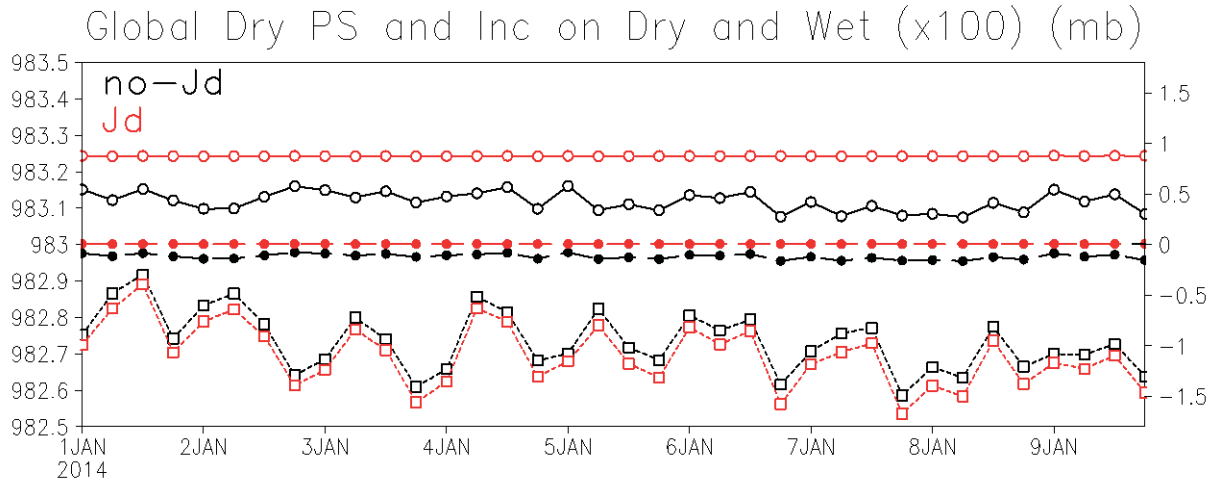


Figure 2.5: Dry-mass and wet-mass time series for two experiments: (i) when a cycled analysis is constrained to conserve dry mass (red curves), and (ii) when the analysis is performed without constraint from the background of (i) (black curves). Dry surface pressure is shown by the open circles. Also shown are the analysis increments on dry mass (closed-red and black circles), and analysis increments on mass water content (open squares). Surface pressure scale is shown on the left vertical axis; increment scale is shown on the right vertical axis.

Experimentation suggests that $\gamma = 5 \times 10^4$ is enough to keep dry mass nearly conserved. As an illustration, Fig. 2.5 shows time series of analysis increments for two cases: (i) a cycling experiment in which the analysis includes the constraint on dry mass; and (ii) a set of non-cycling experiments in which the analysis does not include the constraint. In both cases the GSI analyses see exactly the same background states, and in both cases, the GEOS-5 AGCM producing the background fields conserves dry mass following the modifications of Section 2a. The figure shows analyzed dry mass as the open-circle lines; we see that without the constraint (black) the analysis does not maintain a constant dry mass, whereas it does when the constraint is applied (red), keeping it at the set value of 983.24 hPa. The dry and wet contributions to the mass increment are shown by the closed-circle-dashed and open-square-dotted curves, respectively. Over the short 9-day period considered here, we see that without the dry-mass constraint the analyzed dry-mass changes as the water content increment changes (black). The more physically desirable behavior is shown by the red curves, with the dry mass left unchanged and only the wet contribution varying.

Also pertinent to the present discussion is the fact that the moisture control variable used in the most recent version of GSI (and in the upcoming MERRA-2) is different from that used in its MERRA version. The latter used the so-called pseudo-relative humidity (RH; Dee and da Silva, 2003) whereas the former uses normalized RH (Holm 2003). As it turns out, independent examination finds that pseudo-RH makes humidity increments more sensitive to use of the AMSU-A window channels (pers. comm. William McCarty and Andrea Mold). These channels are used in both MERRA and NCEP-CFSR, with both using the same pseudo-RH humidity control variable choice. This sensitivity is noticeable in the E-P time series shown in Fig. 1.3, and the jump around the end of 1998 corresponds to when the first AMSU-A instrument, on NOAA-15, became available (see table 1 in Rienecker et al., 2011). Indeed, neither ERA-Interim nor JRA-55 shows the jump and sensitivity – in the case of ERA-Interim, not only is the control variable normalized RH, but also the near-surface and window channels, 1-4 and 15, of AMSU-A are not used (Dee et al., 2011).

2c) Adjustment to the Incremental Analysis Update:

In a traditional implementation of an intermittent assimilation cycle, the analysis provides a correction to the model initial condition. In this case, with the model conserving dry mass and with the analysis constrained to allow only changes in the water content that are consistent with the change in total mass, the two features discussed in Sections 2a and 2b keep dry mass nearly unchanged. However, the GEOS-5 ADAS uses the incremental analysis update (IAU) method of Bloom, et al. (1996). Instead of correcting the initial condition, IAU turns the analysis increment into a tendency term that is applied to the model during the assimilation cycle. In

this context, the assimilation in GEOS-5 quickly fails to conserve dry mass given the constancy of the surface pressure and moisture increments over the 6-hour assimilation window. In addition, as shown in Section 1, analysis increments of globally integrated mass and moisture that fail to vanish may lead to imbalances between globally integrated evaporation and precipitation. As a result, globally integrated precipitation amounts become very susceptible to changes in the observational database used by the analysis. Therefore, the IAU procedure has been modified such that the globally integrated analysis increments of mass and moisture vanish, thereby constraining globally integrated dry mass to be conserved. It should be noted that this modification forces all trends in global mass and water content to be driven purely by the model physics, and are only indirectly influenced by the analyzed states of temperature, wind, moisture, and pressure.

Following the procedure used in IAU, we begin with the addition of a constant analysis increment of surface pressure and moisture at every timestep within the 6-hour analysis cycle. At each time-step we compute the smallest departure from the prescribed increment (in a least-squares sense) that will produce vanishing global integrals of the increments. Defining the two functionals, I_p and I_q , which measure the globally integrated squared departure from initial values plus the strong constraints of vanishing increments, we have:

$$I_p = \int \frac{1}{2} \left[\frac{p^{n+1} - p^*}{\alpha} \right]^2 dA + \lambda_p \int (p^{n+1} - p^n) dA$$

$$I_q = \iint \frac{1}{2} \left[\frac{q^{n+1} - q^*}{\beta} \right]^2 dA dp^* + \lambda_q \left[\iint q^{n+1} dA dp^{n+1} - \iint q^n dA dp^n \right].$$

Here p^n and q^n represent the surface pressure and moisture of the background at time n , p^* and q^* represent the surface pressure and moisture that **would** be produced by adding the original GSI analysis increments Δp and Δq , and p^{n+1} and q^{n+1} represent the target values satisfying the constraints. Scaling variables α and β are introduced for generality. Solving the above system through minimization of I_p and I_q yields:

$$p^{n+1} = p^* - \alpha^2 \lambda_p$$

$$q^{n+1} = q^* - \beta^2 \lambda_q$$

$$\lambda_p = \frac{\int (p^* - p^n) dA}{\int \alpha^2 dA}$$

$$\lambda_q = \frac{\iint q^* dA dp^{n+1} - \iint q^n dA dp^n}{\iint \beta^2 dA dp^{n+1}} .$$

While various options were evaluated, choosing scaling variables defined by:

$$\alpha^2 = p^*$$

$$\beta^2 = q^*$$

yields the simple solutions:

$$p^{n+1} = p^* \left(\frac{\overline{p^n}}{\overline{p^*}} \right)$$

$$q^{n+1} = q^* \left(\frac{\int \overline{q^n} dp^n}{\int \overline{q^*} dp^{n+1}} \right) .$$

Here $\overline{(\quad)}$ represents global horizontal integrals. These updated and constrained values of pressure and moisture will now be used in a series of GEOS-5 ADAS experiments to examine their impact on dry mass conservation and P & E balance.

3) Experimental Design

3a) ADAS Evaluation

The model and analysis updates described in Section 2 have been incorporated for use in a series of GEOS-5 ADAS experiments. As a baseline for these tests, data were taken from an interim reanalysis prior to MERRA-2 called GMAO RPIT (Lucchesi, R., 2013), which ran from January 1980 through December 2011. As shown in Fig. 3.1, the GMAO RPIT reanalysis exhibits dramatic changes in globally integrated precipitation due to changes in the satellite observing systems during this time. The nature of jumps such as the one seen in 2008 is not the same as the jump seen in MERRA (top panel of Fig. 1.3); here the window channels of AMSU-A are not used, and GSI uses normalized RH for its humidity control variable. Though not yet fully diagnosed, the jump in precipitation in Fig. 3.1 is most likely associated with the Infrared Atmospheric Sounding Interferometer (IASI) on the METOP-A satellite, which was introduced in the RPIT experiment at the beginning of August 2008. Whatever the reason, the fact remains that the default settings in the GEOS-5 ADAS used for RPIT make the water behavior too

sensitive to changes in the observing system. The RPIT experiment provides a good case study for our purposes here, and we therefore begin this section with a more detailed examination of the RPIT reanalysis for two periods in particular: March 2003 and March 2009.

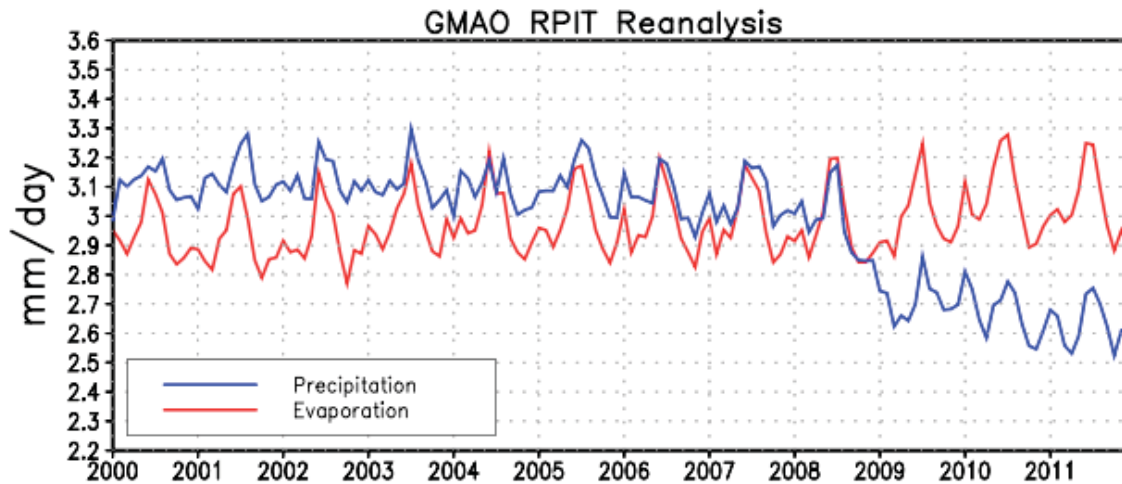


Figure 3.1: Monthly mean globally integrated precipitation and evaporation from the GMAO RPIT Reanalysis .

Figure 3.2 depicts the globally integrated surface pressure (together with its wet and dry components) based on hourly data from the RPIT reanalysis for the months of March 2003 and March 2009. Two issues are readily apparent: 1) a lack of total correlation between the total and wet surface pressures, and 2) a close correlation between the total and dry surface pressure anomalies. The lack of correlation (issue 1) is related to inconsistencies between the analysis increment of surface pressure and the vertically integrated analysis increment of moisture (see Figure 3.3) such that their globally integrated values do not match:

IAU Tendency	March 2003	March 2009
$d(PS)/dt$	0.000908	-0.000306
$d(QINT)/dt$	0.183114	-0.239858

Table 3.1: Globally integrated analysis increments of surface pressure (PS) and column water (QINT) in units of hPa/day.

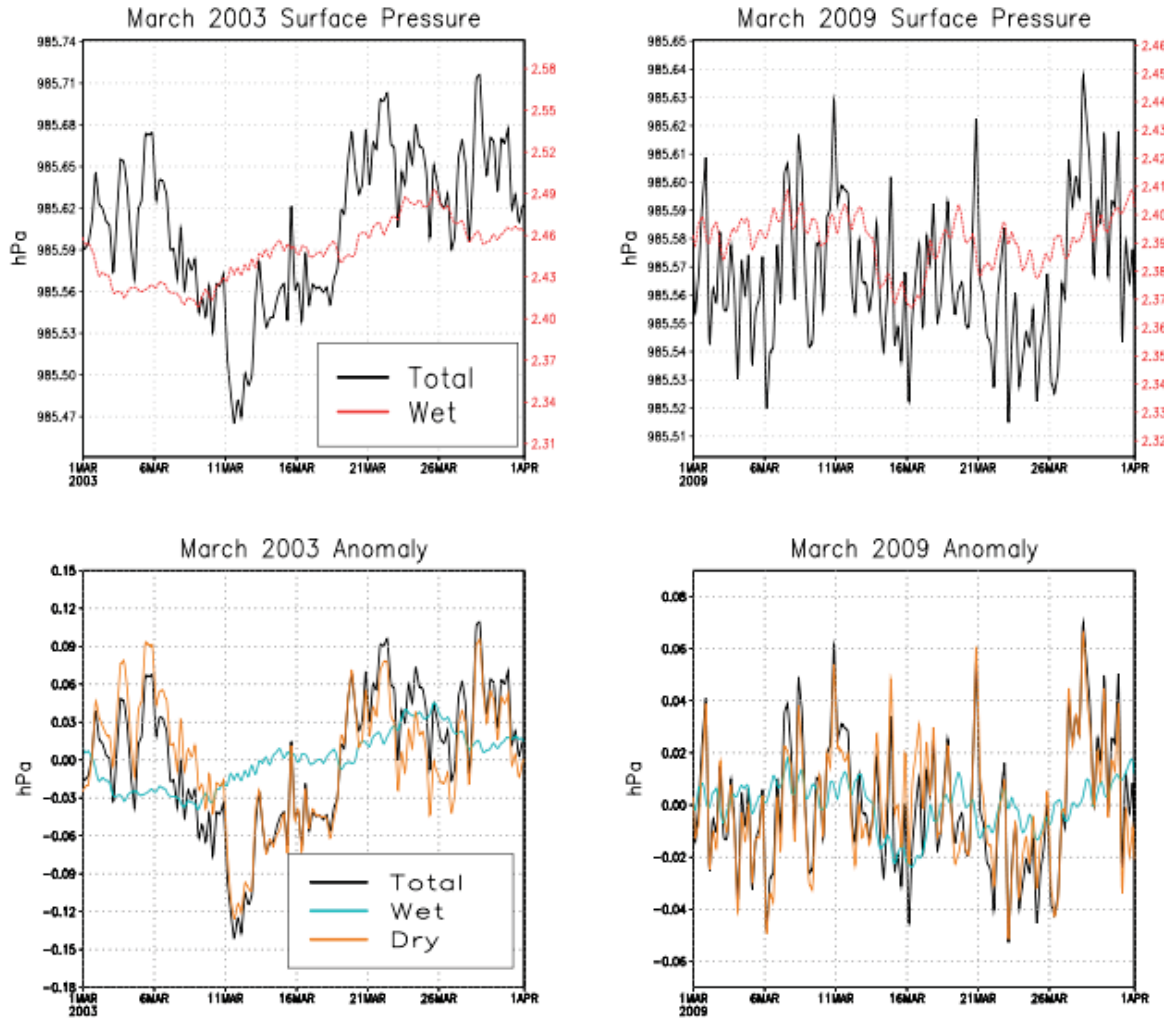


Figure 3.2: Globally integrated surface pressure and its wet and dry partitions from the GMAO RPIT Reanalysis for March 2003 and March 2009.

Figure 3.4 shows the hourly time-series of the globally integrated precipitation and evaporation from the GMAO RPIT reanalysis for the two periods: top panel for March 2003; middle panel for March 2009. It is interesting to note that the mean value of surface evaporation is just under 2.9 mm/day for **both** periods while the mean precipitation value ranges from 3.1 mm/day in March 2003 to 2.6 mm/day in March 2009. Since the total vertically integrated water budget is physically based on the E-P difference, the implied water tendency is quite large for these two periods (shown in the bottom panel of 3.4 using 24-hour running means) with significant non-zero monthly means. The actual vertically integrated precipitable water tendency, however, is much smaller with near-zero monthly means. This difference between actual and implied water tendency is due to the influence of the observationally-based analysis increments and

illustrates the degree to which analysis increments may influence precipitation amounts during data assimilation reanalyses.

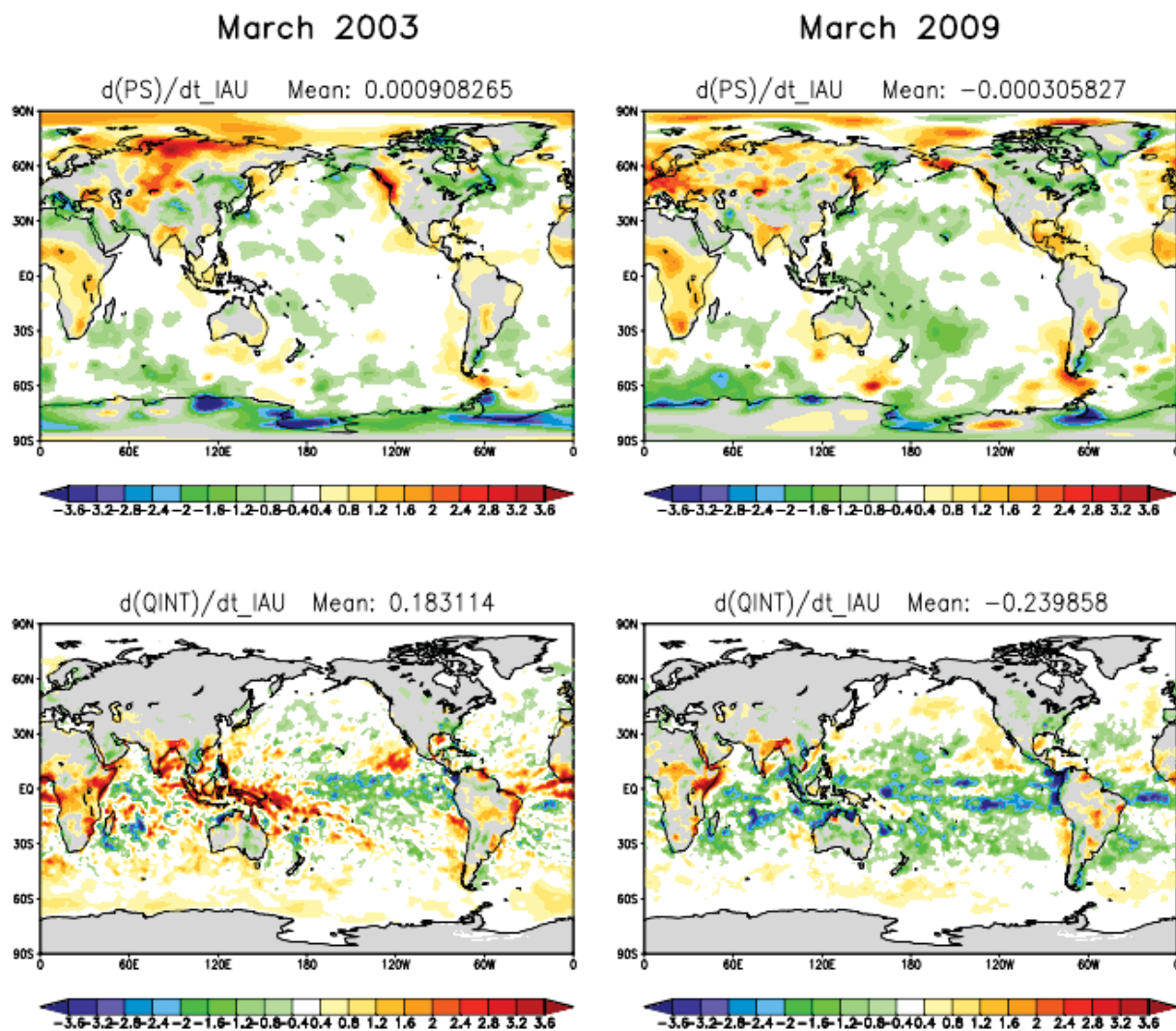


Figure 3.3: Monthly mean analysis increments of surface pressure and vertically integrated moisture (in hPa/day) from the GMAO RPIT reanalysis for the periods March 2003 and March 2009.

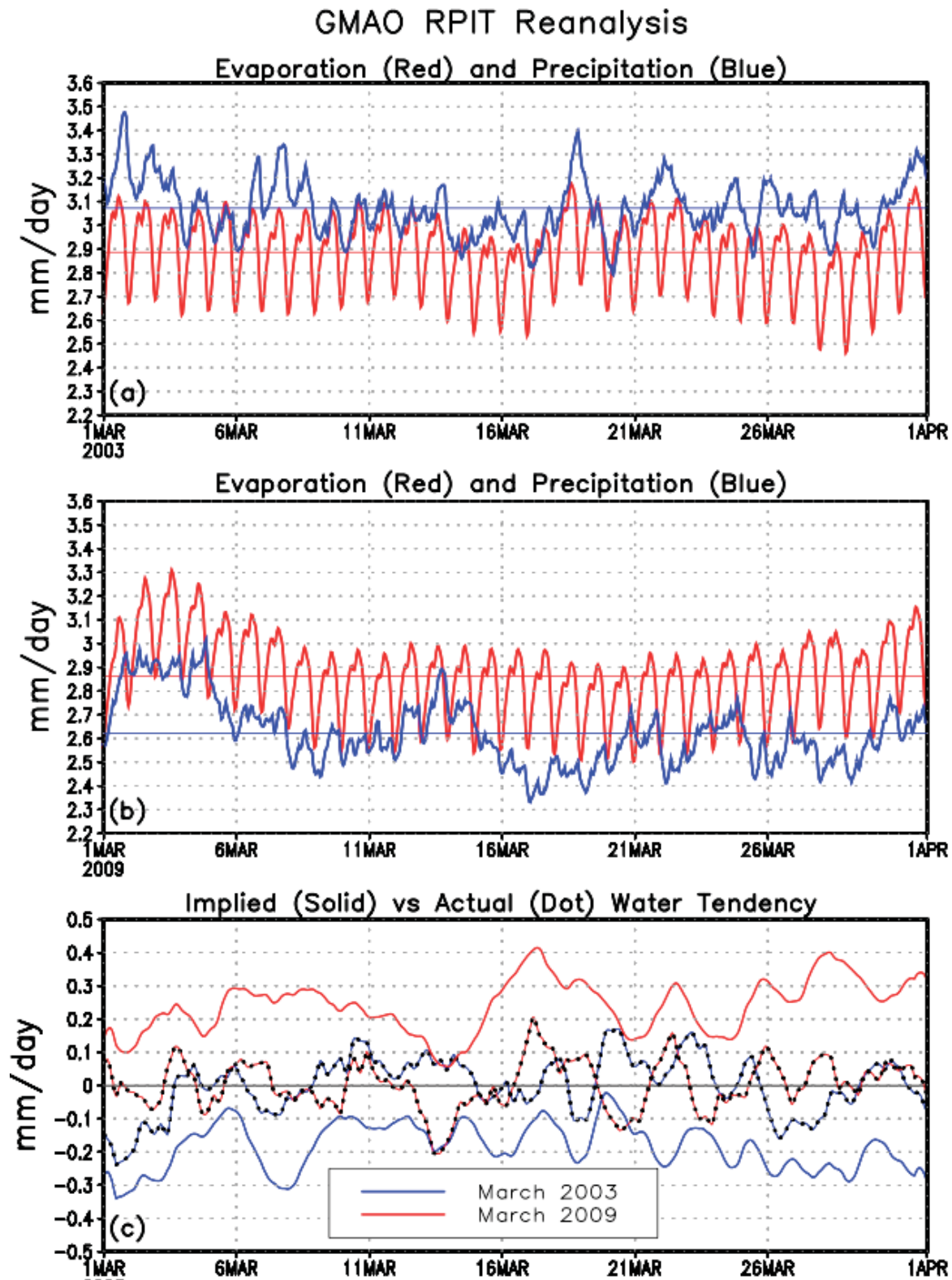


Figure 3.4: Globally integrated evaporation and precipitation from the GMAO RPIT Reanalysis for March 2003 (a) and March 2009 (b). Also shown (c) is the implied (E-P) vs actual water tendency.

Greater insight may be gained by examining the vertical structure of the zonal mean analysis and convective and large-scale moisture tendencies. Figure 3.5 shows the monthly mean, zonal mean moisture tendencies from the two time periods as well as their difference. We see that the structure of the analysis tendency from IAU is significantly different between the two years. In March 2009, the removal of moisture in the upper levels (~500 hPa) due to the analysis is much stronger than in March 2003. As a result, removal by model convection and large-scale processes during March 2009 is significantly impacted resulting in a drop in total precipitation. In addition, the analysis tendency in lower levels (~850 hPa) is significantly greater in March 2003 than in March 2009. It is difficult for the model to retain the additional moisture and, as a result, it is rained out by convective and large-scale processes. Both of these features tend toward producing more precipitation during March 2003 compared to March 2009. This is consistent with the time-series of total precipitation shown in Fig. 3.4.

We have now seen that by failing to constrain the GMAO RPIT reanalysis to conserve dry mass and by allowing non-vanishing global integrals of moisture and surface pressure increments, the GEOS-5 ADAS produces inconsistencies between total and wet surface pressure (due to spurious sources and sinks of dry mass) as well as analysis moisture increments which dramatically impact moist physical parameterizations within the model. Following the development in Section 2, we reran each period using the updated GEOS-5 ADAS (together with a preliminary version of the observational database targeted for the GMAO MERRA-2 reanalysis) using two separate configurations:

- a) Experiment ADAS-1: This configuration (without global constraints) employs the update to the GSI analysis (thereby penalizing increments which produce deviations in dry mass) together with the AGCM update for pressure changes due to moist physics. Conservation of dry mass is not guaranteed since the IAU procedure is not modified.
- b) Experiment ADAS-2: This configuration (with global constraints) employs the GSI and model updates as well as the assimilation update, thereby ensuring conservation of dry mass and vanishing globally integrated pressure and moisture increments.

Both of these configurations use normalized RH for the GSI humidity control variable. In each case, a two week spin-up is used with February 15 initial conditions from the GMAO RPIT reanalysis.

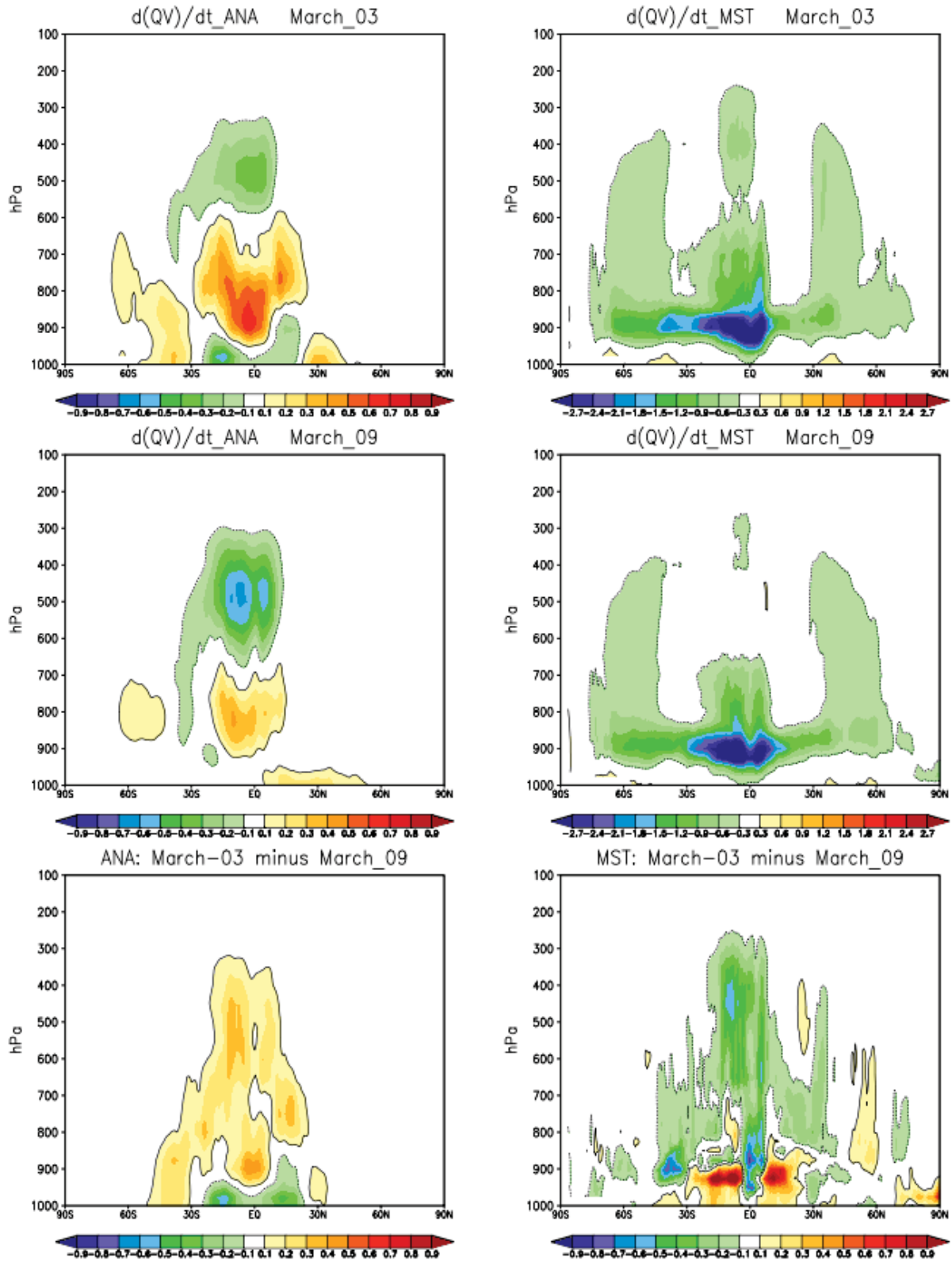


Figure 3.5: Zonal mean moisture tendencies (g/kg/day) from the analysis (ANA; left column) and convective and large-scale rain (MST; right column) from the GMAO RPIT Reanalysis for March 2003 and March 2009. Bottom panels show differences.

Figure 3.6 depicts the globally integrated surface pressure (together with its wet and dry components) based on hourly data from Experiment ADAS-1 for the months of March 2003 and March 2009, while Fig. 3.7 shows results from Experiment ADAS-2. Within ADAS-1 we see that the GSI penalty on globally integrated dry mass departures has made a significant impact toward improving dry mass conservation and consistency between total and wet surface pressure tendencies. The original IAU procedure of Bloom et al. (1996) amounts to a constant tendency during the assimilation period and is thus not able to completely conserve total dry mass.

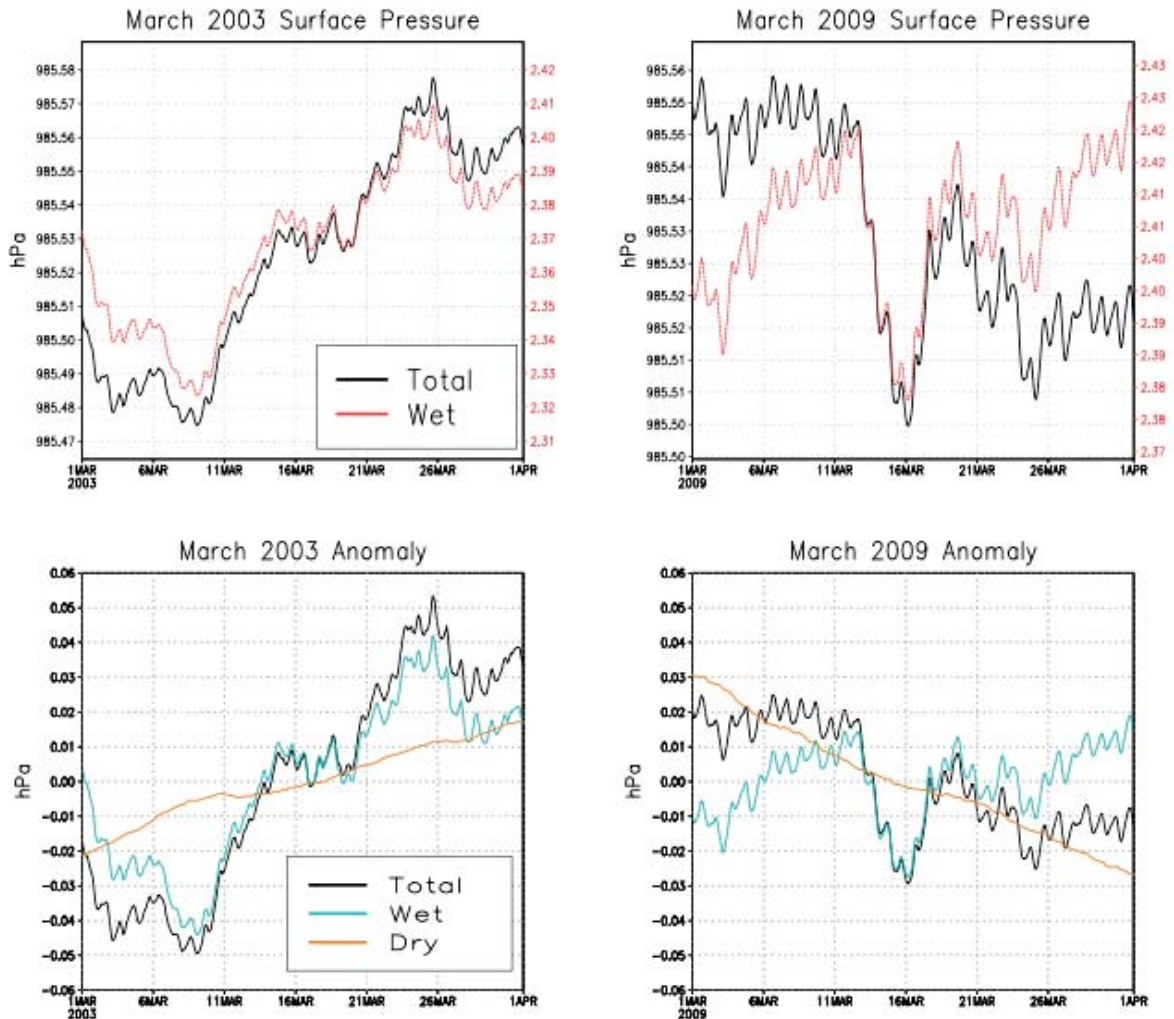


Figure 3.6: Globally integrated surface pressure and its wet and dry partitions from Experiment ADAS-1 (without Constraints) for March 2003 and March 2009.

With the modified IAU strategy discussed in Section 2c, we see perfect conservation of globally integrated dry mass in ADAS-2 (Fig. 3.7). Note that the tendency of wet surface pressure is nearly identical between the ADAS-1 and ADAS-2 experiments. Only the dry mass values have been significantly affected. This is important since the GSI analysis is allowed to influence the total water content of the atmosphere in ADAS-1 (i.e., no restrictions on globally integrated increments) while total water content is purely model-driven in ADAS-2. This is illustrated more clearly when looking at the globally integrated total precipitable water vapor (Fig 3.8).

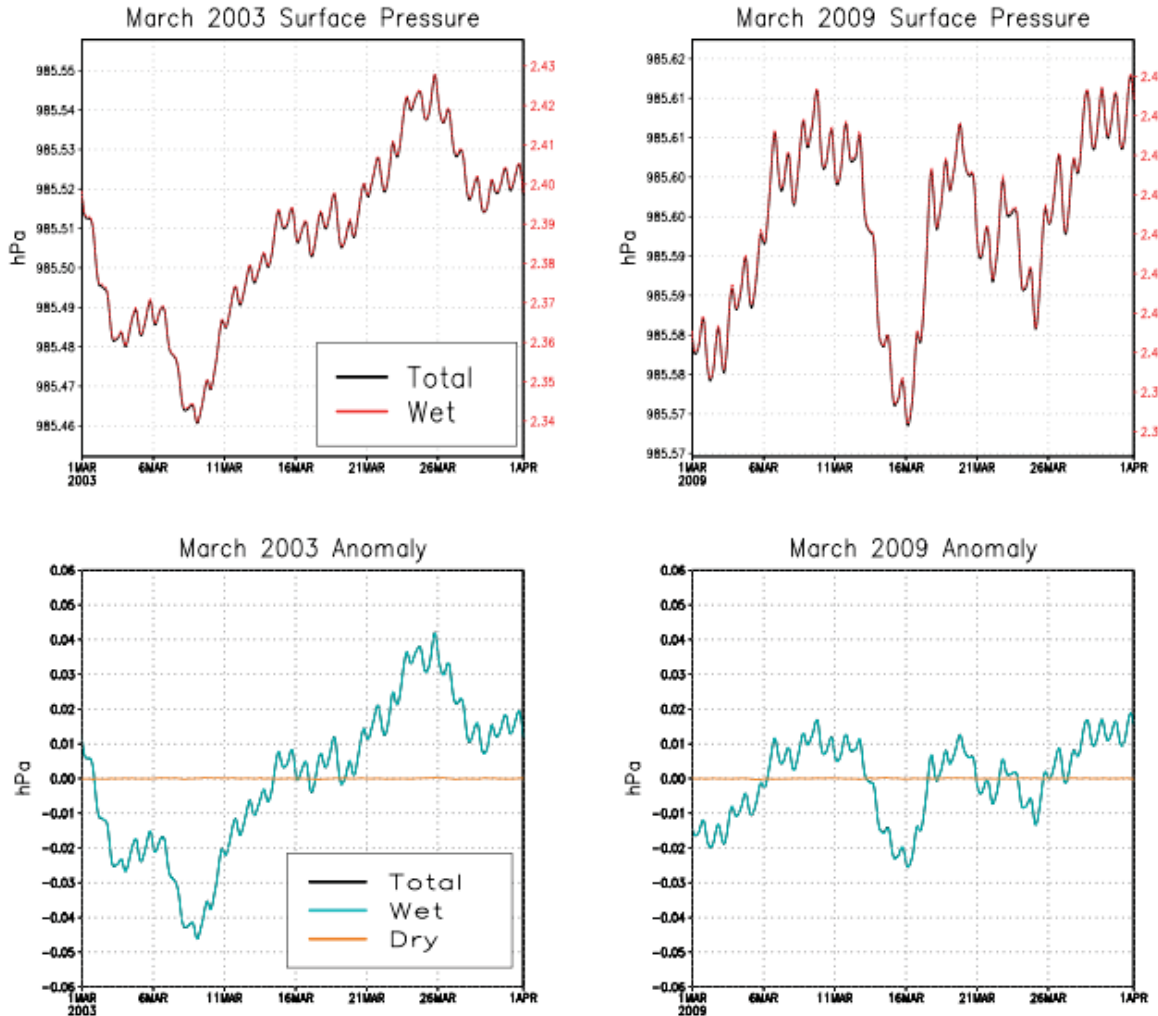


Figure 3.7: Globally integrated surface pressure and its wet and dry partitions from Experiment ADAS-2 (with Constraints) for March 2003 and March 2009.

Here we see that the difference between the two experiments (i.e., with and without global constraints) is smaller than the difference between either run and the original GMAO RPIT reanalysis.

In the early part of the 2003 period (top panel of Fig. 3.8) we see that with the more recent version of GEOS ADAS (used for ADAS-1 and ADAS-2), the two experiments showed a spin up (down) behavior for total precipitable water that differs from that seen in RPIT. This is attributed to a combination of model, analysis, and observing system changes that seem to affect the 2003 period more than 2009 (bottom panel of same figure).

Figures 3.9 and 3.10 show the hourly time-series of the globally integrated precipitation and evaporation from, respectively, ADAS-1 and ADAS-2. In these experiments there is less contrast between the March 2003 and March 2009 periods with respect to values of precipitation. We still see, however, a significant difference between the implied and actual vertically integrated water tendency within ADAS-1, indicating that the analysis increments still contribute significantly to global budgets. Within ADAS-2, the implied and actual water tendencies are in perfect agreement due to the constraint of vanishing global integrals of vertically integrated moisture increments.

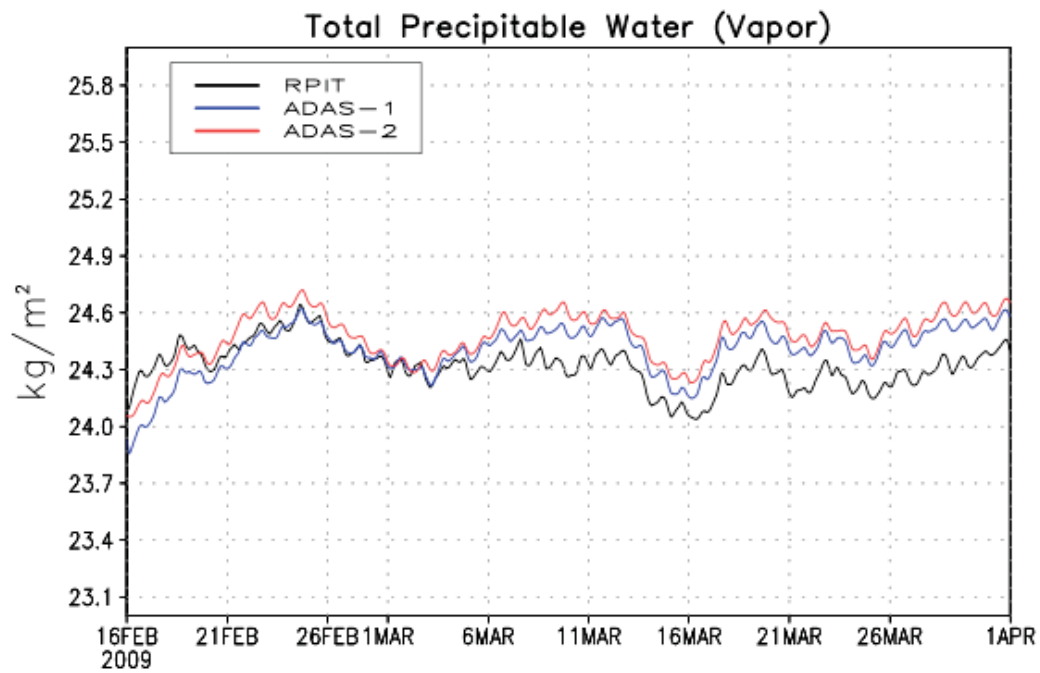
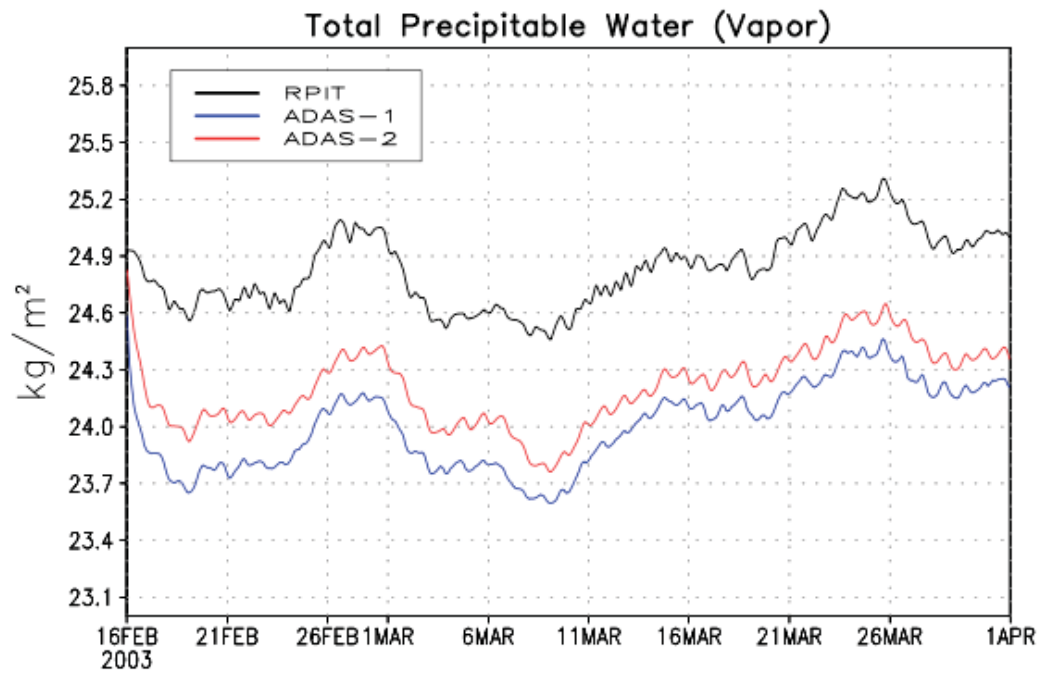


Figure 3.8: Globally integrated total precipitable water from GMAO RPIT as well as from Experiments ADAS-1 (without Constraints) and ADAS-2 (with Constraints) for March 2003 (top) and March 2009 (bottom).

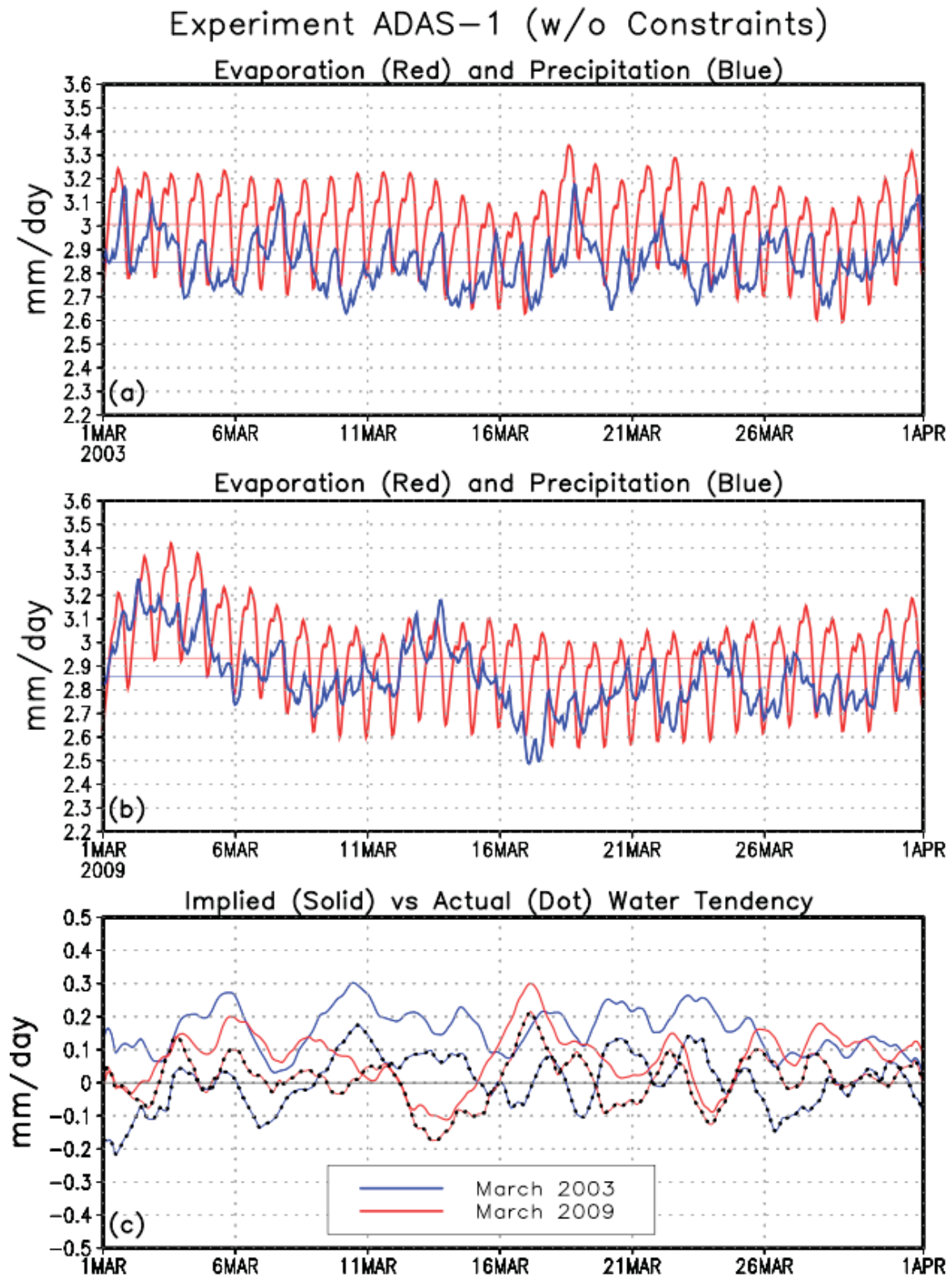


Figure 3.9: Globally integrated evaporation and precipitation from Experiment ADAS-1 for March 2003 (a) and March 2009 (b). Also shown (c) is the implied (E-P) vs actual water tendency.

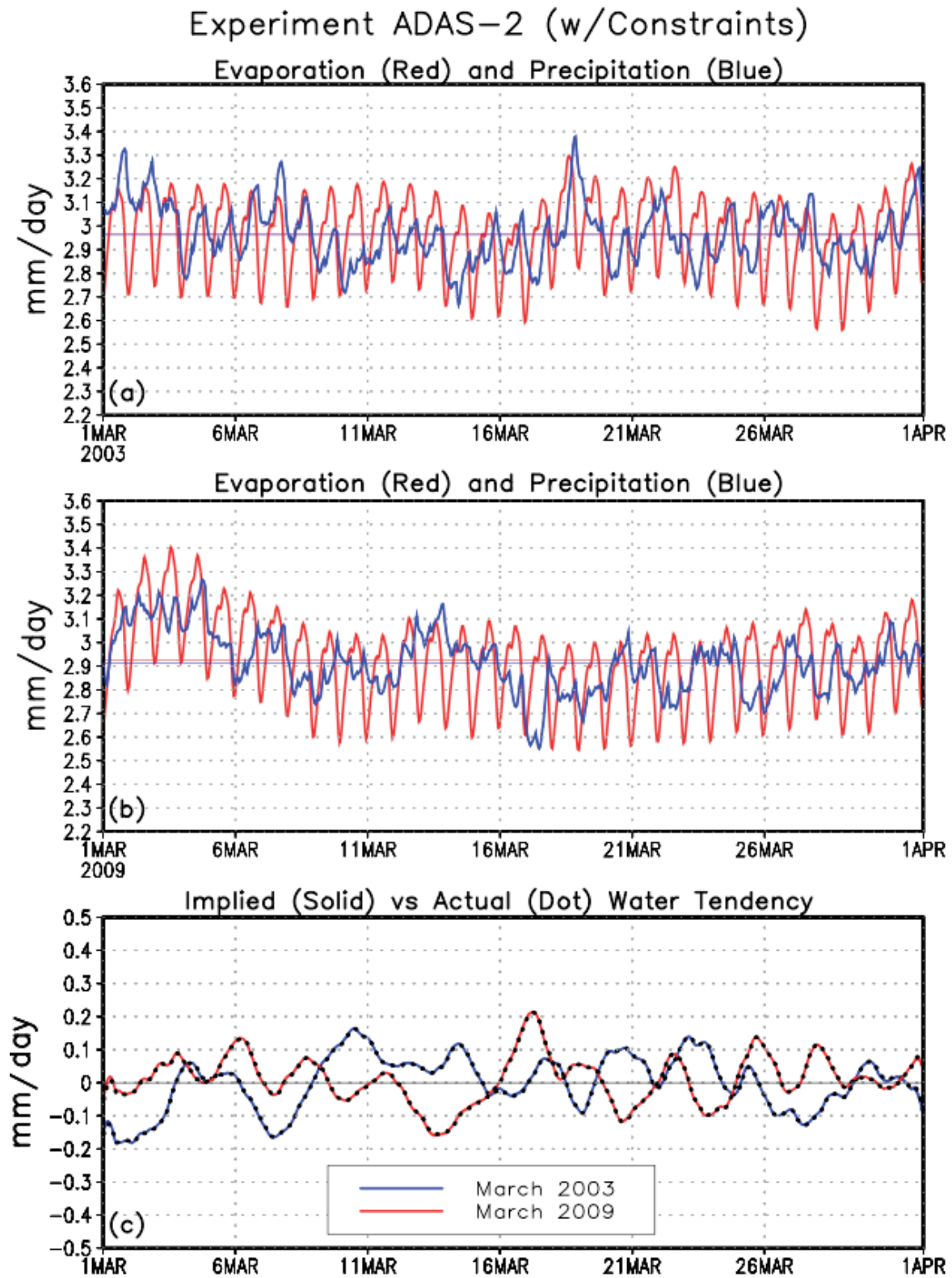


Figure 3.10: Globally integrated evaporation and precipitation from Experiment ADAS-2 for March 2003 (a) and March 2009 (b). Also shown (c) is the implied (E-P) vs actual water tendency.

3b) REPLAY Evaluation

From the results in Section 3a we have seen that the modified IAU procedure produces a conservation of globally integrated dry atmospheric mass as well as a physically-based balance between globally integrated evaporation and precipitation. As a result, the time-series of globally integrated P and E become less sensitive to changes in the observational satellite database used during the assimilation (cf. Figure 3.1) and, therefore, should be more reliable for studies of long-term trends and interannual variability.

To examine this impact in an expedient manner we employ the “REPLAY” option within the GEOS-5 AGCM. The REPLAY mechanism is similar to the standard GEOS-5 ADAS procedure in the sense that it uses IAU to force the assimilation. REPLAY is different from the standard GEOS-5 ADAS in that it uses *pre-existing* analyses to produce IAU increments. The assimilation produced from using REPLAY is thus a blend of the given analysis combined with the atmospheric model in use. This mechanism has been shown to reproduce the original analysis quite well. A singular advantage of REPLAY is that the model used may be different from that originally employed to generate the analysis. In both the GEOS-5 ADAS and the GEOS-5 AGCM with REPLAY, analysis increments are produced and used to force the model during the so-called IAU Corrector step (see Rienecker, et al., 2011). REPLAY may thus be used by modelers as a first step toward correcting systematic biases revealed through an examination of the IAU increments and toward understanding the possible impact of model changes in the data assimilation system.

Using this mechanism, we REPLAY the GMAO RPIT reanalysis from January 2000 through December 2011 using the updated GEOS-5 AGCM (targeted for MERRA-2) under configurations similar to those described in Section 3a (i.e., with and without the global constraints imposed on the IAU increments of p and q). For the REPLAY without global constraints we also removed the model update providing pressure changes from moist physics (thereby mimicking the RPIT configuration more precisely).

Figure 3.11 shows the climatology and monthly mean anomalies of the globally integrated mass and its partition into dry and wet components from the REPLAY without global constraints. Running in this configuration is comparable to the procedure used in the original GMAO RPIT reanalysis that contained no mechanism for dry mass conservation. Results from the REPLAY run are essentially identical to those from the original GMAO RPIT analysis (not shown). We again observe (top panel) a lack of total correlation between the climatological seasonal of total (black curve) and wet (cyan curve) mass, as well as a spurious dry mass anomaly (bottom

panel, orange curve).

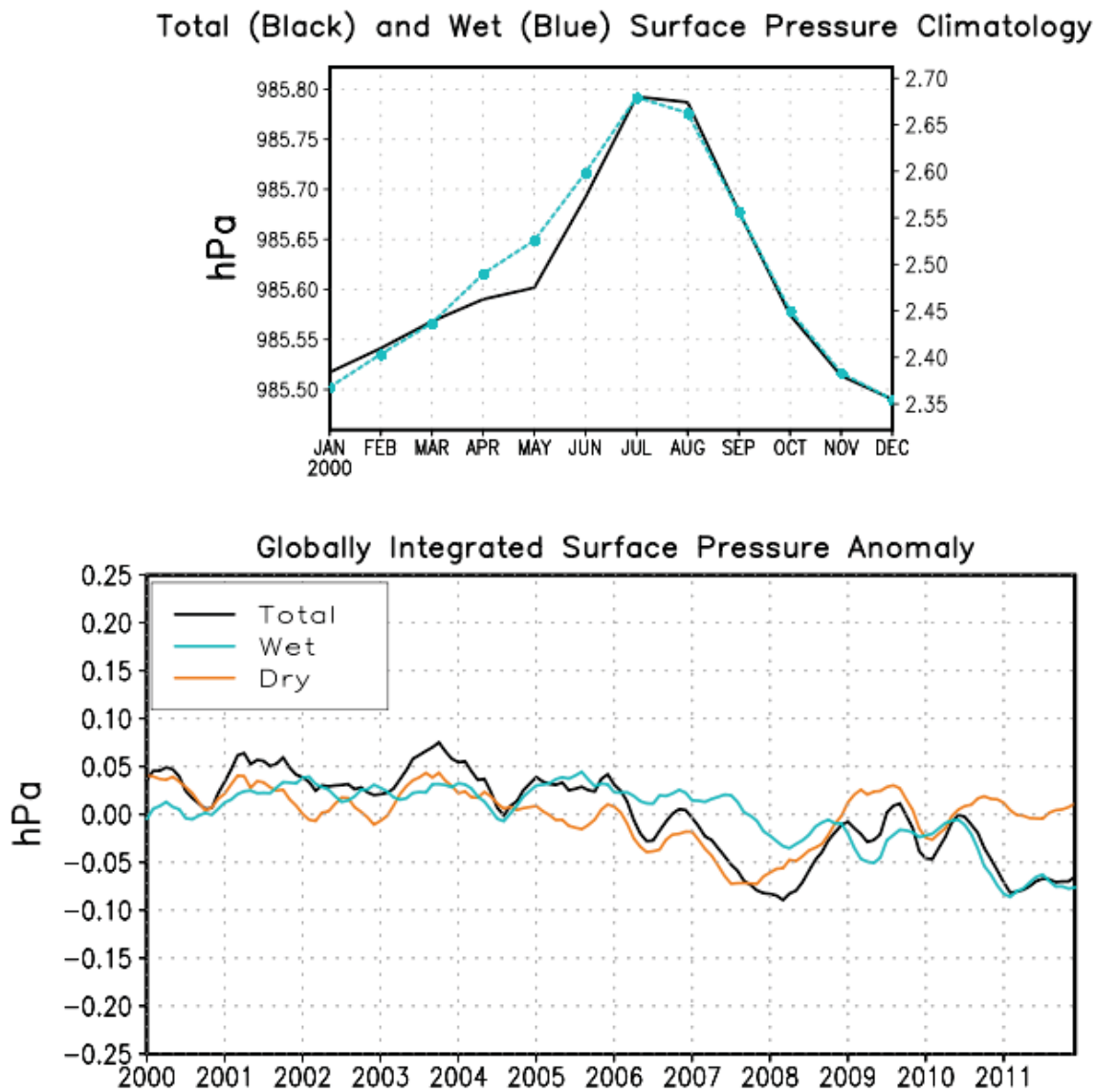
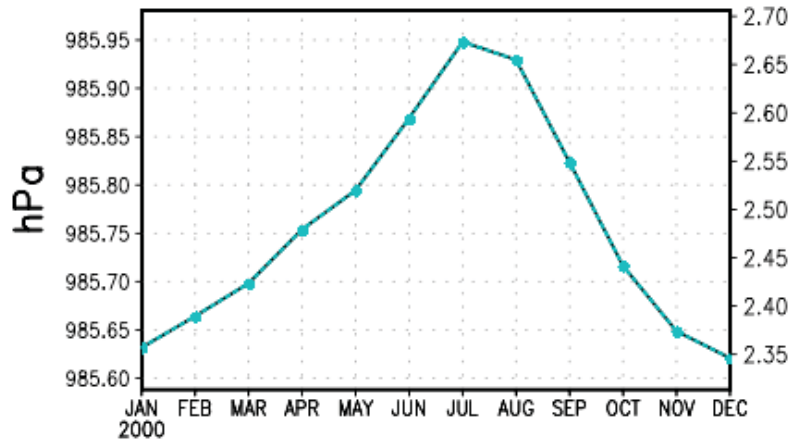


Figure 3.11: Climatology and monthly mean anomalies of globally integrated mass from the GEOS5-AGCM REPLAY of the RPIT Reanalyses. This REPLAY did not use global constraints.

Figure 3.12 shows the same result but for the REPLAY with the global constraints invoked. Here we see that dry mass is perfectly conserved during the run, giving rise to a perfect correlation between the total and wet climatological seasonal cycles (top) and anomalies (bottom). Because the REPLAY assimilation is not allowed to influence the fixed analysis, we see that the trend in the wet component very nearly matches the trend in the REPLAY without constraints.

Total (Black) and Wet (Blue) Surface Pressure Climatology



Globally Integrated Surface Pressure Anomaly

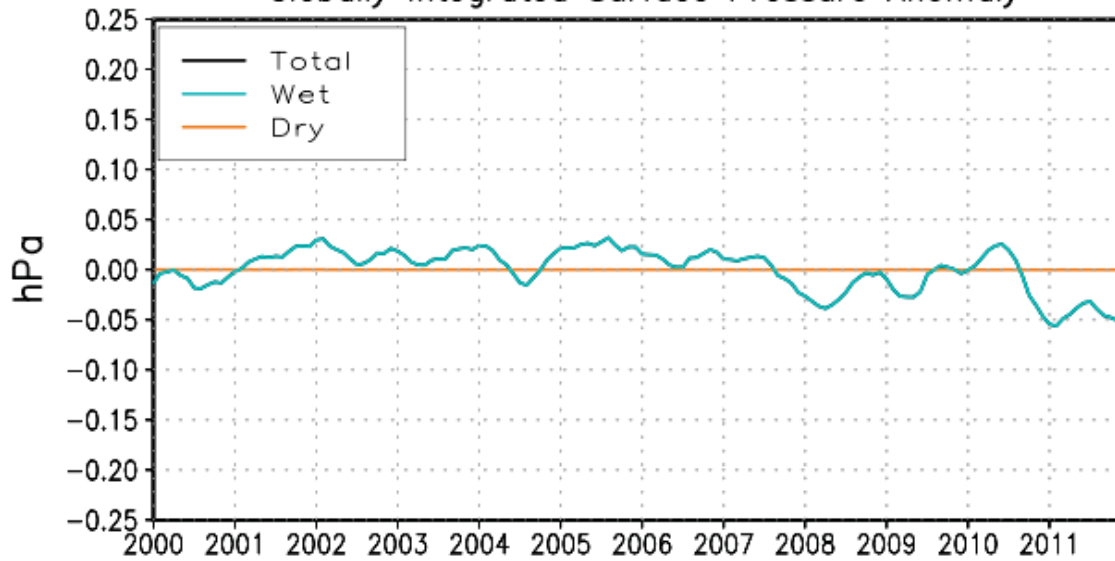


Figure 3.12: Climatology (top: black curve for total; cyan for wet) and monthly mean anomalies (bottom: black for total; cyan for wet; and red for dry) of globally integrated mass from the GEOS5-AGCM REPLAY of the RPIT reanalyses (note, black and cyan curves completely overlay). This REPLAY did use global constraints.

Figure 3.13 repeats the plot for the globally integrated precipitation and evaporation from the GMAO RPIT reanalysis in addition to showing results from the two REPLAY experiments. We see that REPLAY without global constraints produces the same signature with respect to the P and E balance as does RPIT. There are small differences in precipitation amounts compared

with RPIT due to model updates targeted for MERRA-2, but the overall character is the same. The REPLAY with global constraints, as expected, shows a perfect balance between P and E.

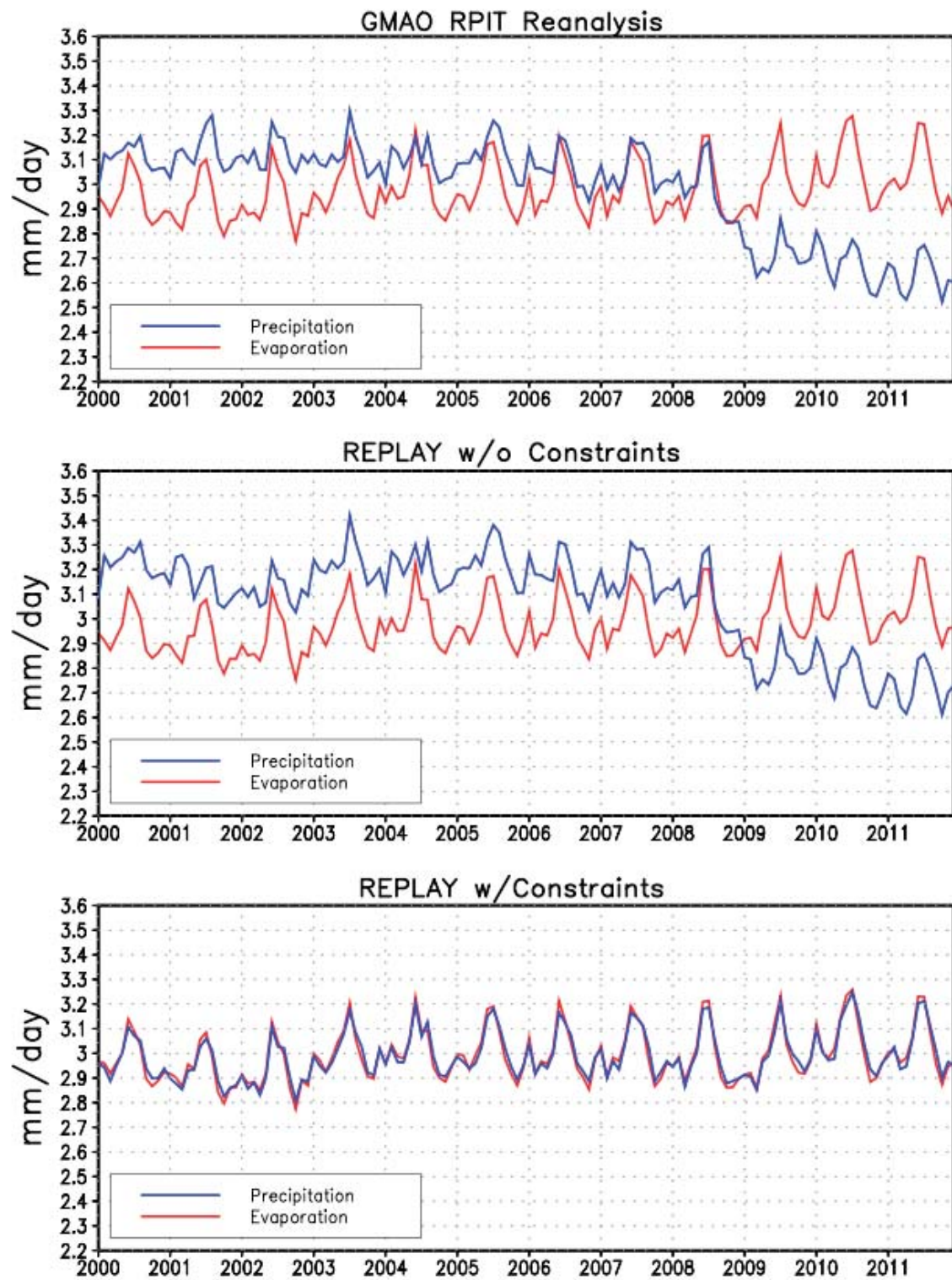


Figure 3.13: Globally integrated evaporation and precipitation from the GMAO RPIT reanalysis and the two REPLAY experiments (with and without constraints).

4) Preliminary MERRA-2 Results

The GMAO MERRA-2 was started in the spring of 2014. While not yet complete, we show here some preliminary results which have incorporated all updates previously discussed. The MERRA-2 Reanalysis is being carried out through four concurrently-running operational streams (initialized in January of 1979, 1991, 2000, and 2010). The following figures show results from each of the four streams.

Figure 4.1 shows the time series of total surface pressure separated into its dry and wet components. We see that each stream is conserving its initial globally-integrated dry mass value of 983.24 hPa (surface pressure equivalent). The wet surface pressure component shows the well defined seasonal cycle associated with total water content.

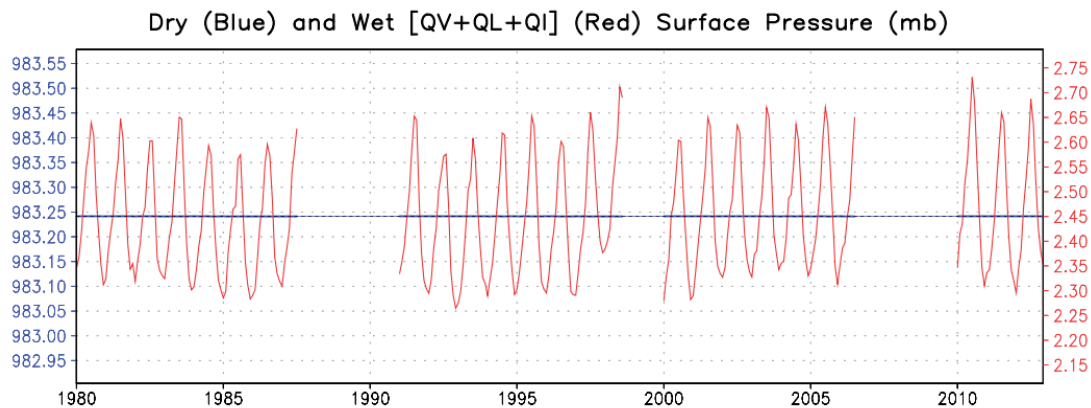


Figure 4.1: Globally integrated surface pressure separated into its wet and dry components from the GMAO MERRA-2.

Figure 4.2 shows the time series of MERRA-2 globally integrated precipitation and evaporation as well as its comparison to the precipitation produced in MERRA. We see that the MERRA-2 system has a very steady rate of precipitation compared to that from MERRA. In addition, the precipitation from MERRA-2 is in balance with the MERRA-2 evaporation (cf. Fig. 1.1). The addition of global mass and water vapor constraints within the ADAS has greatly reduced the sensitivity of MERRA-2 to changes in the observational database.

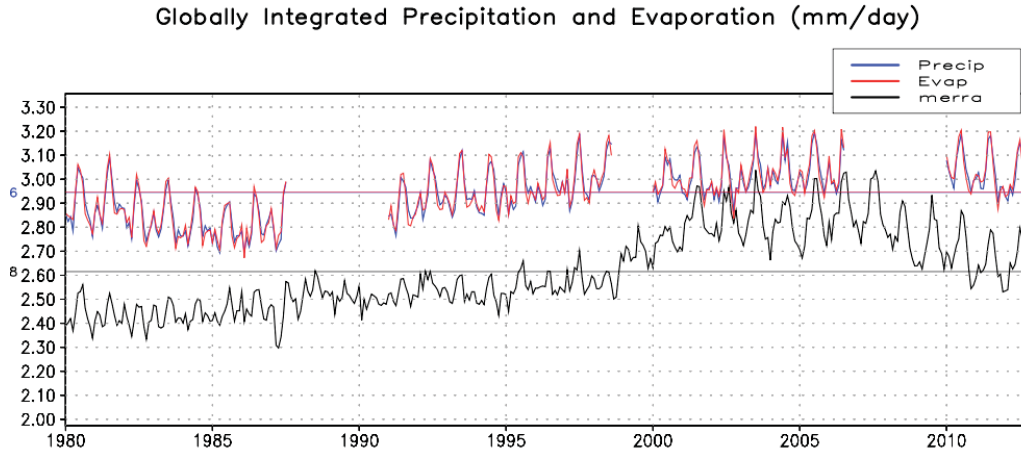


Figure 4.2: Globally integrated precipitation and surface evaporation from MERRA-2, and its comparison to MERRA precipitation (in black).

As a final preliminary examination we look at the time series of globally integrated total precipitable water (TPW). As indicated earlier, the globally integrated value of total water content is now entirely model-driven due to the constraint of vanishing globally integrated analysis moisture increments. In ADAS mode the magnitude of TPW is directly governed by model physics and only indirectly constrained by the analyzed fields (wind, temperature, moisture, and pressure). Therefore it is instructive to compare total water content values to an independent observational dataset to determine if model moisture bias too strongly influences total water content. For this purpose we use data from the Goddard Satellite-based Surface Turbulent Fluxes project (GSSTF version 2b, Shie et al. 2009) covering the period from 1987 through 2008 measured over oceans. Figure 4.3 shows the time-series *departure* from GSSTF of total precipitable water from two streams within the MERRA-2 ADAS system covering the GSSTF time period and averaged over the oceanic regions consistent with GSSTF. The mean value of GSSTF over this period is $\sim 2.8 \text{ g/cm}^2$. As a comparison we also show the total precipitable water departure as computed from a 30-year $\frac{1}{2}$ -deg AMIP simulation initialized in February 1979 using the MERRA-2 model as well as the results from the MERRA-1 ADAS. We see that while the MERRA-2 model tends to run wet in AMIP mode, the magnitude of total precipitable water in ADAS mode is in close agreement with the GSSTF-based data. The results from the MERRA-1 ADAS again show the sensitivity of the moisture variable to changes in the observational/satellite network.

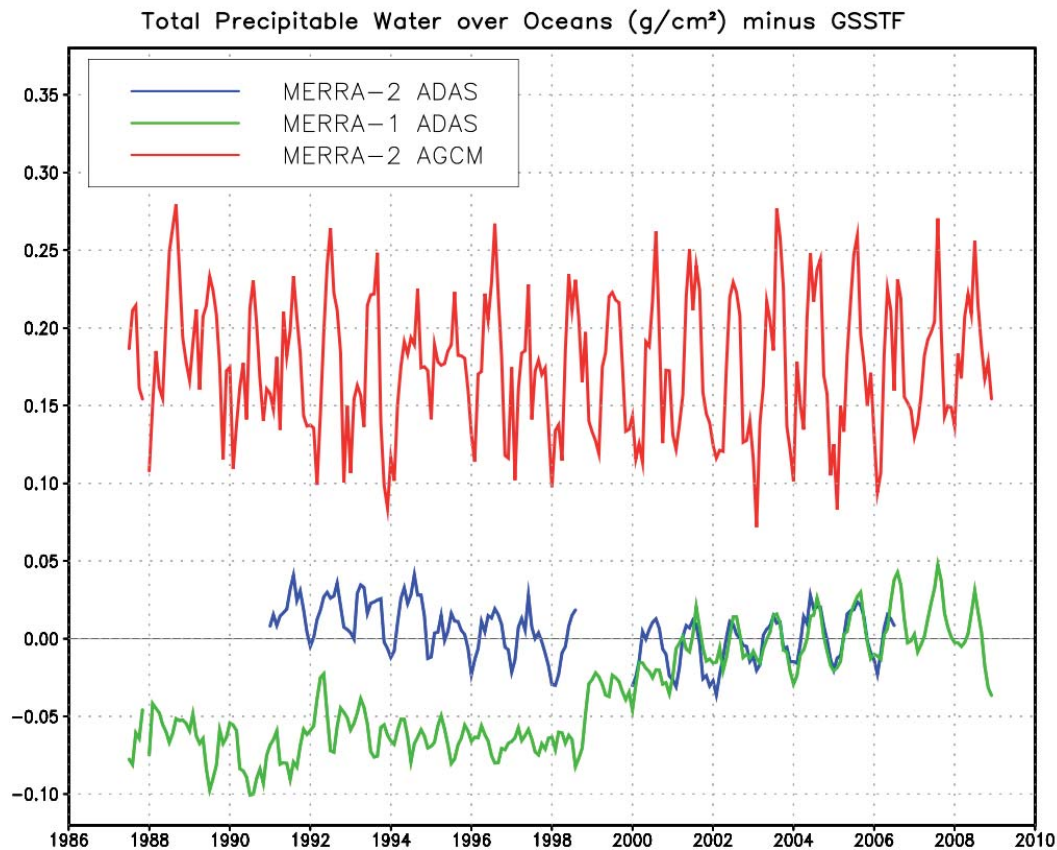


Figure 4.3: Globally integrated total precipitable water from MERRA-1 ADAS, MERRA-2 ADAS, and MERRA-2 AGCM compared with GSSTF.

5) Summary

In this report we have shown that recent reanalysis efforts have generated imbalances between globally integrated precipitation and surface evaporation. These imbalances are due to the observationally-based analysis adjustments, which are highly sensitive to changes in the observational/satellite database. In addition to this water imbalance, we have seen that there is a lack of correlation between trends in total surface pressure and trends in total water content. In fact, most of the trend in total surface pressure comes from a spurious trend in the dry mass. An effort has been made in this study to modify the atmospheric model, the GSI analysis, and the IAU assimilation procedure such that globally integrated dry mass is conserved and such that precipitation and surface evaporation are in model balance. Experiments have shown that the resulting modified algorithm conserves dry mass and substantially lessens the impact of changes in the observational database on precipitation.

Acknowledgement

The authors thank their GMAO colleagues for discussions in group meetings throughout the development of this work, in particular: Stephen Bloom, Ronald Gelaro, William McCarty, and Andrea Molod. We also thank Atanas Trayanov for help with some implementation details. Experiments were carried out using the Linux cluster of the NASA Center for Climate Simulation.

6) References

- Bloom, S., L. Takacs, A. DaSilva, and D. Ledvina, 1996: Data assimilation using incremental analysis updates. *Mon. Wea. Rev.*, **124**, 1256-1271.
- Bosilovich, M.G., and F.R. Robertson, 2011: Global Energy and Water Budgets in MERRA. *J. Climate*, **24**, 282-300.
- Dee, D. P., and A. M. da Silva, 2003: The choice of variable for atmospheric moisture analysis. *Mon. Wea. Rev.*, **131**, 155-171.
- Dee, D. P., and 35 co-authors, 2011: The ERA-Interim reanalysis: Configuration and performance of the data assimilation system. *Quart. J. R. Meteorol. Soc.*, **137**, 553-597. DOI: 10.1002/qj.828.
- Derber, J. C., and A. Rosati, 1989: A global oceanic data assimilation system. *J. Phys. Oceanography*, **19**, 1333-1347.
- Ebita, A., S. Kobayashi, Y. Ota, M. Moriya, R. Kumabe, K. Onogi, Y. Harada, S. Yasui, K. Miyaoka, K. Takahashi, H. Kamahori, C. Kobayashi, H. Endo, M. Soma, Y. Oikawa, and T. Ishimizu, 2011: The Japanese 55-year Reanalysis "JRA-55": an interim report, SOLA, **7**, 149-152.
- El Akkraoui, A., Y. Tremolet, and R. Todling, 2013: Preconditioning of variational data assimilation and the use of a bi-conjugate gradient method. *Quart. J. R. Meteorol. Soc.*, **139**, 731-741.
- Hoinka, K. P., 1998: Mean global surface pressure series evaluated from ECMWF reanalysis data. *Q.J.R. Meteorol. Soc.*, **124**, 2291-2297.
- Holm, E. V., 2003: Revision of the ECMWF humidity analysis: Construction of a Gaussian control variable. *Proc. Workshop on Humidity Analysis*, Reading, U.K., ECMWF/GEWEX, 1-6. [Available online from <http://old.ecmwf.int/publications/library/ecpublications/pdf/workshop/2002/Humidity/holm.pdf>]
- Kleist, D. T., D. F. Parrish and J. C. Derber and R. Treadon and W.-S. Wu and S. Lord, 2009: Introduction of the GSI into the NCEP's Global Data Assimilation System. *Wea. Forecasting*, **24**, 1691-1705.
- Lucchesi, R., 2013: File Specification for GEOS-5 FP-IT. GMAO Office Note No. 2 (Version 1.2), 60pp, available from http://gmao.gsfc.nasa.gov/pubs/office_notes.

Massart, S., B. Pajot, A. Piacentini, and O. Pannekoucke, 2010: On the merits of using 3D-FGAT assimilation scheme with an outer loop for atmospheric situations governed by transport. *Mon. Wea. Rev.*, **138**, 4509-4522.

Reynolds, R.W., N.A. Rayner, T.M. Smith, D.C. Stokes, and W. Wang, 2002: An improved in situ and satellite SSA analysis for climate. *J. Climate*, **15**, 1609-1625.

Rienecker, M.M., M.J. Suarez, R. Gelaro, R. Todling, J. Bacmeister, E. Liu, M.G. Bosilovich, S.D. Schubert, L. Takacs, G.-K. Kim, S. Bloom, J. Chen, D. Collins, A. Conaty, A. da Silva, et al. (2011), MERRA: NASA's Modern-Era Retrospective Analysis for Research and Applications. *J. Climate*, **24**, 3624-3648, doi:10.1175/JCLI-D-11-00015.1.

Saha, S., and Coauthors, 2010: The NCEP Climate Forecast System Reanalysis. *Bull. Amer. Meteor. Soc.*, **91**, 1015–1057. doi: <http://dx.doi.org/10.1175/2010BAMS3001.1>

Shie, C.-L., L.S. Chiu, R. Adler, E. Nelkin, I.-I. Lin, P. Xie, F.C. Wang, R. Chokngamwong, W. Olson, and D.A. Chu, 2009: A note on reviving the Goddard satellite-based surface turbulent fluxes (GSSTF) dataset. *Adv. Atmos. Sci.*, **26(6)**, 1071-1080.

Trenberth, K.E., 1991: Climate Diagnostics from Global Analyses: Conservation of Mass in ECMWF Analyses. *J. Climate*, **4**, 707-722.

Trenberth, K.E., J.R. Christy, and J.G. Olson, 1987: Global Atmospheric Mass, Surface Pressure, and Water Vapor Variations. *J. Geophys. Res.*, **92**, 14815-14826.

Trenberth, K.E., and C. Guillemot, 1994: The total mass of the atmosphere. *J. Geophys. Res.*, **99**, 23079-23088.

Trenberth, K.E., and L. Smith, 2005: The Mass of the Atmosphere: A Constraint on Global Analysis. *J. Climate*, **18**, 864-875.

